https://doi.org/10.5194/acp-2022-517
Preprint. Discussion started: 9 August 2022

Atmospheric Chemistry and Physics Discussions

Effects of transport on a biomass burning plume from Indochina during EMeRGe-Asia identified by WRF-Chem

Chuan-Yao Lin[1]*, Wan-Chin Chen[1], Yi-Yun Chien[1], Charles C. K. Chou[1], Chian-Yi Liu[1], Helmut Ziereis[2], Hans Schlager[2], Eric Förster[3], Florian Obersteiner[3], Ovid O. Krüger[4], Bruna A. Holanda[4], Mira L. Pöhlker[4,a], Katharina Kaiser[5,7], Johannes Schneider[5], Birger Bohn[8] , Maria Dolores Andrés Hernández[6], John P. Burrows[6]

1. Research Center for Environmental Changes, Academia Sinica, Taipei, Taiwan
2. Deutsches Zentrum für Luft- und Raumfahrt (DLR), Institut für Physik der Atmosphäre, Oberpfaffenhofen, Germany
3. Karlsruhe Institute of Technology, Institute of Meteorology and Climate Research, Karlsruhe, Germany
4. Multiphase Chemistry Department, Max Planck Institute for Chemistry, Mainz, Germany
5. Particle Chemistry Department, Max Planck Institute for Chemistry, Mainz, Germany
6. Institute of Environmental Physics, University Bremen, Bremen, Germany
7. Institute for Atmospheric Physics, Johannes Gutenberg University, Mainz, Germany
8. Institute of Energy and Climate Research IEK-8, Forschungszentrum Jülich, Jülich, Germany

[a]now at: Faculty of Physics and Earth Sciences，Leipzig Institute for Meteorology, University of Leipzig/Experimental Aerosol and Cloud Microphysics Department, Leibniz Institute for Tropospheric Research, Leipzig, Germany

*Corresponding author
Chuan Yao Lin,
Research Center for Environmental Changes, Academia Sinica, Taipei, Taiwan
128 Sec. 2, Academia Rd, Nankang, Taipei 115, Taiwan
(E-mail: yao435@rcec.sinica.edu.tw, Tel.: +886-2-27875892, Fax: +886-2-27833584),

Abstract.

https://doi.org/10.5194/acp-2022-517
Preprint. Discussion started: 9 August 2022


Atmospheric Chemistry and Physics Discussions

The Indochina biomass burning (BB) season in springtime has a substantial environmental impact on the surrounding areas in Asia. In this study, we evaluated the environmental impact of a major long-range BB transport event on 19 March 2018 (a flight of the HALO research aircraft, flight F0319) preceded by a minor event on 17 March 2018 (flight F0317). Aircraft data obtained during the campaign in Asia of the Effect of Megacities on the transport and transformation of pollutants on the Regional to Global scales (EMeRGe) were available between 12 March and 7 April 2018. In the F0319, results of 1-min mean carbon monoxide (CO), ozone (O_3), acetone (ACE), acetonitrile (ACN), organic aerosol (OA) and black carbon aerosol (BC) concentrations were up to 312.0 ppb, 79.0 ppb, 3.0 ppb, 0.6 ppb, 6.4 µg m^{-3}, 2.5 µg m^{-3} respectively, during the flight, which passed through the BB plume transport layer (BPTL) between the elevation of 2000–4000 m over the East China Sea (ECS). During F0319, CO, O_3, ACE, ACN, OA and BC maximum of the 1 minute average concentrations were higher in the BPTL by 109.0 ppb, 8.0 ppb, 1.0 ppb, 0.3 ppb, 3.0 µg m^{-3} and 1.3 µg m^{-3} compared to flight F0317, respectively. Sulfate aerosol, rather than OA, showed the highest concentration at low altitudes (<1000 m) in both flights F0317 and F0319 resulting from the continental outflow in the ECS.

The transport of BB aerosols from Indochina and its impacts on the downstream area was evaluated using a WRF-Chem model. Over the ECS, the simulated BB contribution demonstrated an increasing trend from the lowest values on 17 March 2018 to the highest values on 18 and 19 March 2018 for CO, fine particulate matter ($PM_{2.5}$), OA, BC, hydroxyl radicals (OH), nitrogen oxides (NO_x), total reactive nitrogen (NO_y), and O_3; by contrast, the variation of $J(O^1D)$ decreased as the BB plume's contribution increased over the ECS. In the low boundary layer (<1000 m), the BB plume's contribution to most species in the remote downstream areas was <20 %. However, at the BPTL, the contribution of the long-range transported BB plume was as high as 30–

https://doi.org/10.5194/acp-2022-517
Preprint. Discussion started: 9 August 2022

Atmospheric Chemistry and Physics Discussions

80 % for most of the species (NO_y, NO_x, $PM_{2.5}$, BC, OH, O_3, and CO) over South China (SC), Taiwan, and the ECS. BB aerosols were identified as a potential source of cloud condensation nuclei, and the simulation results indicated that the transported BB plume had an effect on cloud water formation over SC and the ECS on 19 March 2018. The combination of BB aerosol enhancement with cloud water resulted in a reduction of incoming shortwave radiation at the surface in SC and the ECS which potentially has significant regional climate implications.

1 Introduction

Biomass burning (BB) is one of the main sources of aerosols, greenhouse gases, and air pollutants (e.g. Ramanathan et al., 2007; Lin et al., 2009; 2014; Tang, 2003; Carmichael et al., 2003; Chi et al., 2010; Fu et al., 2012; Lin N.H. et al., 2012; Chuang et al., 2016). Reid et al. (2013) and Giglio et al. (2013) investigated the seasonal aerosol optical depth over Southeast Asia and have indicated that Indochina is a major contributor of carbon emissions in springtime. Galanter et al. (2000) estimated that BB accounts for 15–30 % of the entire tropospheric CO background. Huang et al. (2013) indicated that the contribution of BB in Southeast Asia to the aerosol optical depth (AOD) in Hong Kong and Taiwan could be in the range of 26-62 %. Moreover, BB emissions over Indochina are a significant contributor to black carbon (BC), organic carbon (OC), and O_3 in East Asia (Lin et al., 2014). In their BB modeling study, Lin et al. (2014) identified a northeast (NE) to southwest (SW) zone stretching from South China (SC) to Taiwan with a reduction in shortwave radiation of approximately 20 W m^{-2} at the ground surface. In addition, the total carbon emission from BB in Southeast Asia is approximately 91 Tg C yr^{-1}, accounting for 4.9 % of the global total (Yadav et al., 2017). According to Xu et al. (2018), BB in Indochina leads to BC production at high

https://doi.org/10.5194/acp-2022-517
Preprint. Discussion started: 9 August 2022


Atmospheric Chemistry and Physics Discussions

concentrations of up to 2–6 μg m^{-3} in spring. The authors reported that BC particles were transported to the glaciers in the Tibetan Plateau, where it significantly affected the melting of the snow, causing some severe environmental problems, such as water resource depletion. Ding et al. (2021) indicated that BB aloft aerosols strongly increase the low cloud coverage over both land and ocean and affect the monsoon in the subtropical Southeast Asia.

Although many researchers have indicated the importance of BB emissions, their precise estimation and applying in the modeling study remains challenging (Fu et al. 2012; Huang et al. 2013; Pimonstree et al. 2018; Marvin et al. 2021). For example, Heald et al. (2003) conducted an emission inventory in Southeast Asia and reported that the uncertainties of BB emission estimations could be a factor of three or even higher. Following an inverse model analysis, Palmer et al. (2003) also indicated the overestimation of regional BB emissions over Indochina. Shi and Yamaguchi (2014) pointed out BB emissions exhibited similar temporal trends between 2001 and 2010 and with strong interannual variability over southeast Asia. Satellite data can be used to easily locate hotspots such as those where agricultural residuals burning and forest wildfires are occurring worldwide. However, accurately quantifying the amount of BB emission from satellite data is difficult because anthropogenic pollutants and BB emissions are typically mixed in the atmosphere. During the NASA Transport and Chemical Evolution over the Pacific (TRACE-P) aircraft mission in spring 2001, Jacob et al. (2003) observed that warm conveyor belts (WCBs) lift both anthropogenic and BB (from SE Asia) air pollution to the free troposphere, resulting in complex chemical signatures. Wiedinmyer et al. (2011) demonstrated that the uncertainty of emission estimation could be as high as a factor of 2 because of the error introduced by estimates in fire hotspots, area burned, land cover maps, biomass consumption, and emission factors in the model. In this context, Lin et al. (2014) highlighted the uncertainty of

https://doi.org/10.5194/acp-2022-517
Preprint. Discussion started: 9 August 2022


Atmospheric Chemistry and Physics Discussions

emission estimation in the first version of Fire Inventory from NCAR (Wiedinmyer et al., 2011).

The transport of BB pollution is strongly dependent on the atmospheric structure and weather conditions. Tang et al. (2003) noted that most BB aerosols, having their source in Indochina (mainly south of 25 °N and be alofted to an altitude of 2000–4000 m) during the TRACE-P campaign were associated with outflow in the WCB region after frontal passage. Lin et al. (2009) suggested a mountain lee-side troughs as an important mechanism, resulting in BB product transport from the surface to >3000 m. BB pollution is often transported from its sources to the East China Sea (ECS), Taiwan, and the western North Pacific within a few days.

The airborne field experiment EMeRGe (Effect of Megacities on the transport and transformation of pollutants on the Regional to Global scales) over Asia was led by the University of Bremen, Germany and conducted in collaboration with Academia Sinica, during the inter-monsoon period in 2018 (http://www.iup.uni-bremen.de/emerge/home/home.html). The EMeRGe aircraft mission consists of two parts. The first mission phase was conducted in Germany in July 2017 and the second phase was conducted from Taiwan in 2018 (Andrés Hernández et al. 2022).EMeRGe in Asia aimed at the investigation of the long range transport (LRT) of local and regional pollution originating in Asian major population centers (MPCs) from the Asian continent into the Pacific. A central part of the project was the airborne measurement of pollution plumes on-board of the High Altitude and Long Range Research Aircraft (HALO). The HALO platform was based in Tainan, Taiwan (Fig. 1a-b), and made optimized transects and vertical profiling in regions north or south of Taiwan, dependent on the relevant weather and emission conditions. HALO measurements additionally provide important information for the evaluation of the LRT of BB emissions and its potential environmental impact in East Asia between 12 March and 7

https://doi.org/10.5194/acp-2022-517
Preprint. Discussion started: 9 August 2022


Atmospheric Chemistry and Physics Discussions

April 2018. During the EMeRGe-Asia campaign, HALO carried out 12 mission flights in Asia and 4 transfer flights from Europe to Asia with a total of 110 flight hours.

This paper is organized as follows: the model configuration and BB emission analysis employed in the model simulation are described in Section 2, and the weather conditions and HALO measurement results are presented in Section 3. The model performance, as well as the evaluation of BB product transport and effects on East Asia selected regions are discussed in Sections 4 and 5, respectively.

2 Aircraft data and Model configuration

2.1 HALO aircraft data

The HALO aircraft was equipped with a number of instruments and a detailed description of the measurement systems onboard the HALO was presented in Andrés Hernández et al.(2022). In this study, aerosol data (OA, BC, SO_4^{2-}, NO_3^-, NH_4^+), and trace gases such as CO, SO_2, O_3, NO_x, NO_y, acetone (ACE), acetonitrile (ACN), HCHO, HONO, OH, HO_2, and photolysis rate $J(O^1D)$, $J(NO_2)$ were employed in the analysis.

2.2 WRF-Chem Model and model configuration

We used the Weather Research Forecasting with Chemistry (WRF-Chem) model (Ver. 4.1.1) (Grell et al., 2005) to study the LRT of air masses associated with BB pollutants in Indochina. The initial and boundary meteorological conditions for WRF-Chem were obtained from National Centers for Environmental Prediction (NCEP)-GDAS Global Analysis data sets at 6-h intervals. The Mellor–Yamada–Janjic planetary boundary layer scheme (Janjic, 1994) was applied. The horizontal resolution for the simulations performed was 10 km, and the grid box had 442 × 391 points in the east–west and north–south directions (Fig. 1a). A total of 41 vertical levels were included, with the lowest level at an elevation of approximately 50 m. To improve the accuracy of the meteorological fields, a grid nudging four-dimensional data assimilation scheme was

https://doi.org/10.5194/acp-2022-517
Preprint. Discussion started: 9 August 2022


Atmospheric Chemistry and Physics Discussions

applied using the NCEP-GDAS Global Analysis data.

The cloud microphysics used followed the Lin scheme (Morrison et al., 2005). The rapid radiative transfer model (Zhao et al., 2011) was used for both longwave and shortwave radiation schemes. Moreover, land surface processes are simulated using the Noah-LSM scheme (Hong et al., 2009). In terms of transport processes, we considered advection by winds, convection by clouds, and diffusion by turbulent mixing. The removal processes in this study were gravitational settling, surface deposition, and wet deposition (scavenging in convective updrafts and rainout or washout in large-scale precipitation). The kinetic preprocessor (KPP) interface was used in both of the chemistry schemes of the Regional Atmospheric Chemistry Mechanism (RACM, Stockwell et al., 1990). The secondary organic aerosol formation module, the Modal Aerosol Dynamics Model for Europe (Ackermann et al., 1998)/Volatility Basis Set (Ahmadov et al., 2012), was also employed in the WRF-Chem model. In RACM, "KET" is the only species available for ketones. Thus, we do estimate the measurement of ACE by using simulated KET in this study.

2.3 Emission Inventories

Anthropogenic emissions, such as NO_x, CO, SO_2, nonmethane volatile organic compounds, sulfate, nitrate, PM_{10}, and $PM_{2.5}$, were adopted on the basis of the emission inventory in Asia – MICS-Asia III (Li et al., 2020; Kong et al., 2020). For BB emissions FINNv1.5 (https://www.acom.ucar.edu/Data/fire/) was employed. FINN provided daily, 1000 m resolution, global estimates of the trace gas and particle emissions from open BB, which included wildfires, agricultural fires, and prescribed burning but not biofuel use and trash burning (Wiedinmyer et al., 2011). The anthropogenic emissions in Taiwan were obtained from the Taiwan Emission Data System (TEDS) which is the emission inventory of the air-pollutant monitoring database of the Taiwan

https://doi.org/10.5194/acp-2022-517
Preprint. Discussion started: 9 August 2022


Atmospheric Chemistry and Physics Discussions

Environmental Protection Administration. The TEDS version used for this study was V9.0 (2013) and contained data on eight primary atmospheric pollutants: CO, NO, NO_2, NO_x, O_3, PM_{10}, $PM_{2.5}$, and SO_2.

3 Characteristics of the field experiment

3.1 MODIS Aerosol optical depth and Weather conditions

Figures 2a and b visualizes the numerous fire hotspots and high aerosol optical depth on 17 March 2018 registered by the MODIS satellite. Indeed, a large number of BB fire hotspots frequently occurred over Indochina during the springtime (Lin et al. 2009; 2014) and EMeRGe-Asia campaign (supplementary Figure S1). On 17 March 2018 at 06:00 UTC (14:00 LT; LT = UTC+8:00) the weather data indicated a series of high-pressure systems in northern China and a separate high-pressure system over Korea (Fig. 2c). At 1000 hPa, a strong northerly continental outflow was identified over southern Japan, the ECS, and Taiwan (Fig. 2d). On 19 March 2018, a new frontal system was located from Korea to the Guangdong province in SC (Fig. 2e). On the same day at 06:00 UTC, a discontinued flow was identified at the frontal zone to the north of Taiwan in the ECS (Fig. 2f). In other words, Taiwan was located at the prefrontal and warm conveyor area due to the surrounding southerly flow on 19 March 2018 at 06:00 UTC (Figs. 2e and 2f, respectively). The southerly wind was gradually replaced by the northeasterly after another frontal passage on 20 March 2018 at 00:00 UTC (data not shown).

In the upper layer (700 hPa; Figs. 2g–2j), the flow pattern differed from that at the near-ground surface (1000 hPa; Figs. 2d and 2f). A southwesterly strong wind, coming from the east side of the Tibetan Plateau in SC, moving to the North Eats i.e. Korea, is converted to a polar front wave flow in northeastern China and Korea on 17 March 2018 (Fig. 2g). This high-elevation northward strong wind belt distribution at 700 hPa

https://doi.org/10.5194/acp-2022-517
Preprint. Discussion started: 9 August 2022


Atmospheric Chemistry and Physics Discussions

was associated with a corresponding lee-side trough at the east of the Tibetan Plateau, whereas a ridge was noted over the east coast of China on the same day (Fig. 2h). Consistent with the mechanism reported by Lin et al. (2009), once a significant lee-side trough formed, it provided favorable conditions for the upward motion over the lee-side of the Tibetan Plateau and brought BB emission to the free troposphere layer following the strong wind belt transport to the downwind area. After the weather system moved to the east, the north–south trough turned to SW–NE such that the strong wind belt was in an approximately SW–NE direction and located between 20 and 30 °N on 19 March 2018 (Figs. 2i and 2j). In conclusion, the Indochina BB pollutants were driven by the strong wind belt from Indochina, northward to SC on 17 March 2018 and then eastward passing over Taiwan between 20 and 30 °N to the south of Japan on 19 March 2018.

3.2 Characteristics of LRT BB to the ECS by WRF-Chem model

Figure 3 shows latitude longitude plots of the simulated CO concentration differences with and without BB emission at an elevation of 1000 m (Fig. 3a), mainly in Indochina, SC, and the South China Sea on 17 March 2018. The ambient flow was easterly and then northward from the South China Sea to SC at 1000 m elevation between 00:00 and 12:00 UTC on 17 March 2018 (Fig. 3a-b). The BB plume accumulated and persisted for an extended period in the lower part of the boundary layer on 17 and 19 March 2018 (Figs. 3a-b, and 3e-f). In contrast, the high CO concentration followed the southwesterly or westerly strong wind belt (Figs. 3c-d, and 3g-h) and its weather conditions (Fig. 2) at an elevation of 3000-m (700 hPa). Following the movement of the ridge and trough at the 700 hPa geopotential height (Fig. 2h and 2j), the associated strong wind belt turned to move eastward in the SW–NE direction between 17 and 19 March 2018. The BB plume transport over Indochina was affected by a fast-moving strong flow at 700 hPa (Fig. 2g and 2i), shifting the plume toward Taiwan and the ECS, during 17–19 March 2018. The highest CO concentration

https://doi.org/10.5194/acp-2022-517
Preprint. Discussion started: 9 August 2022


Atmospheric Chemistry and Physics Discussions

contributed by the BB plume was >150 ppb, originally sourced from Indochina, and it was mainly transported northward on 17 March 2018 (Figs. 3c-d) and then covered a large area in East Asia at a CO concentration of >100 ppb on 19 March 2018 (Figs. 3g-h). Figure 4 indicates simulation differences for the contribution of BB along an E–W cross-section at 30 °N at 16:00 UTC on 18 March 2018 (Fig. 4a) and 06:00 UTC on 19 March 2018 (Fig. 4b). We noted that a strong wind at 2000 m elevation and a high CO concentration (>70 ppb) due to BB at the BPTL. Moreover, the CO concentration attributed to BB was low at the elevation of >4000 m on 19 March at 06:00 UTC (Fig. 4b), showing that the BB pollutants mainly affect altitudes below 4000 m.

3.3 Aircraft measurements

Two HALO flights were scheduled to the ECS to measure the pollutants following the continental outflow; the flights departed on 17 (Fig. 5a) and 19 (Fig. 6a) March 2018 and followed similar tracks. To indicate the measurement results along the flight path, the 1-min average data is shown in Figures 5b and 6b. On 17 March 2018, the flight departed from Tainan (Fig. 1b) at 01:09 UTC (09:09 LT) first southbound and then northward to the ECS (Fig. 5a). The elevation for sample collection was mainly <4000 m, where the CO concentration was found to be <200 ppb in most cases on that day (Fig. 5b). At elevations between 2000 and 4000 m, the concentration of the major aerosol components (i.e., OA, BC, SO_4^{2-}, NO_3^-, and NH_4^+) was mostly <2 μg m^{-3}, except just above western Taiwan after 08:00 UTC (Figs. 5a–5d). The peak concentrations for OA, BC, SO_4^{2-}, NH_4^+, and NO_3^- were 3.4, 1.2, 2.1, and 0.7 μg m^{-3}, respectively, at the altitude between 2000 and 4000 m. SO_4^{2-} demonstrated the highest concentration among the aerosol components, especially during 04:00–04:37 and 05:48–06:15 UTC (peaking at 5.1 μg m^{-3}) when the flight was north of 30 °N and an elevation of <1000 m (Figs. 5a–5c). This result could be attributed to anthropogenic pollution from the continental outflow (Lin et al. 2012) or probably part from Japan

https://doi.org/10.5194/acp-2022-517
Preprint. Discussion started: 9 August 2022


Atmospheric Chemistry and Physics Discussions

contributed to the high sulfate concentration in the boundary layer over the ECS. As for the trace gases such as ACE, ACN and O_3, their concentrations between 2000 and 4000 m were stable and ranged between 1-2 ppb, 0.1-0.3 ppb, and 60-70 ppb (Fig. 5b), respectively, implying minor influence over the ECS by the BB plume in this flight. Figure 5e illustrates the HYSPLIT (Stein et al., 2021) 96-h backward trajectories, which identified the air mass origin starting at 02:00 UTC, followed by 04:00, 06:00, and 09:00 UTC. The continental outflow contributed to higher sulfate concentrations (3–5 μg m^{-3} at 33 °N) at 04:00 and 06:00 UTC (Figs. 5b, 5c, and 5e) at <1000 m along the flight path. In contrast, south of 25 °N and above Taiwan, the local pollution and continental outflow are dominating sources on 17 March 2018.

The HALO flight on 19 March 2018 departed at 00:19 UTC (08:19 LT). It was bound northward and sampled air at an altitude of <4000 m most of the time, as shown in Figures 6a and 6b. Figures 6c and 6d indicate the latitude-height variation of SO_4^{2-} and OA mass concentrations along the flight path on 19 March 2018. As the flight left Taiwan, it maintained an elevation of 3000 m during 01:00–02:00 UTC (Fig. 6a, 121–126 °E) and then descended to <1000 m during 02:00–02:40 UTC (Fig. 6b). The OA mass concentration was higher at 3000 m than at the low altitude during 01:00–03:00 UTC (Figs. 6b and 6d). In particular, CO, OA and BC exhibited a substantial peak concentration of 312 ppb, 6.4 μg m^{-3} and 2.5 μg m^{-3} at 01:54 and 02:51 UTC at 26 °N, 125–126 °E, and an altitude of 2000–4000 m, where a BPTL was observed. The trace gases such as ACE, ACN, and even O_3 (Fig. 6b) have consistent peak times in the BPTL with concentrations of 3.0 ppb, 0.6 ppb, and 79 ppb, respectively. In this flight, SO_4^{2-} had the second-highest concentration among the aerosol components (1–2.4 μg m^{-3}; Figs. 6b and 6c) upstream of Taiwan (25–27 °N) during 1:00–3:00 UTC.

In the northern part of the flight between 03:00 and 05:00 UTC at an elevation of >3000 m, the aerosol component concentrations were all at their lowest level (Figs. 6b–

https://doi.org/10.5194/acp-2022-517
Preprint. Discussion started: 9 August 2022


Atmospheric Chemistry and Physics Discussions

296 6d). During 05:00–07:00 UTC, the HALO aircraft flew back southward to 25 °N, where
297 high OA mass concentrations appeared again between 2000 and 4000 m (Figs. 6a, 6b,
298 and 6d). Sulfate was the species with the highest concentration between 05:30 and
299 06:30 UTC (Figs. 6b and 6c) when the flight's elevation was <1000 m in the lower
300 boundary between 25 and 27 °N (upstream of Taiwan). The reason explaining this
301 observation is that the transport of anthropogenic pollutants of continental origin takes
302 place mainly in the boundary layer (Figs. 6b–6d). Other aerosol species, such as NO_3^-
303 and NH_4^+, demonstrated low concentrations, except when the elevation was <1000 m,
304 where they ranged up to 1 μg m^{-3} (Fig. 6b).

305 The 96-h HYSPLIT backward trajectory starting from the flight locations at
306 02:00–07:00 UTC (Fig. 6e) indicated that the air masses at elevations between 2000
307 and 4000 m were potentially transported from Indochina. North of 30 °N and at altitudes
308 of >3000 m at 04:00 UTC, the concentrations of air pollutants (including OA, SO_4^{2-},
309 NO_3^-, and NH_4^+) were low (Figs. 6b and 6e) even though the air mass in the low
310 boundary was sourced from SC and the Taiwan Strait. In general, the results are
311 consistent with those of Lin et al. (2009, 2014), Carmical et al. (2003), and Tang et al.
312 (2003): the BPTL was mainly located south of 30 °N. The fact that higher OA was
313 observed rather in the higher altitudes than in the lower boundary also demonstrated
314 the vertical distribution over the ECS.

315 Figure 7 displays the vertical distribution of the gases and major aerosol
316 components found on the flights on 17 (blue) and 19 (green) March 2018 as well as the
317 mean concentrations noted in the seven flights (on 17, 19, 22, 24, 26, and 30 March and
318 4 April 2018; red) to the ECS during EMeRGe-Asia. Figure 7 illustrates all profiles
319 calculated as 1-min mean and every 500-m interval with one standard deviation (±σ).
320 The number of the data points is displayed on the right side of each figure. The mean
321 CO concentration profile demonstrated a decreasing trend from 240 ppb near the

https://doi.org/10.5194/acp-2022-517
Preprint. Discussion started: 9 August 2022


Atmospheric Chemistry and Physics Discussions

ground to 150 ppb at an altitude of 2500 m and 140–160 ppb at altitudes >6000 m (Fig. 7a). The concentration for 17 March 2018 (flight F0317) was similar to the mean concentration profile, except for that at the <1500 m elevation in the lower boundary. However, a higher CO concentration (40–80 ppb) enhancement was noted on 19 March 2018 (flight F0319) than the mean profile and flight F0317. The mean difference in CO concentration between flights F0319 and F0317 was as high as 80 ppb at an elevation of 3000-3500 m (Fig. 7a). Similarly, OA concentration was significantly higher in the BPTL vertical distribution in flight F0319 than in the mean profile and flight F0317 (Fig. 7b). The mean OA concentration for the flight F0319 peaked at an elevation of 2000–2500 m, increasing to 2 μg m^{-3} more than in the mean profile and flight F0317. Other aerosol components such as SO_4^{2-}, NH_4^+, and NO_3^- (Supplementary Fig. S2a-c) also had a similar vertical distribution trend, but the concentration differences were minor compared with OA concentrations. The magnitude of the maximum differences between the flights F0319 and F0317 in the BPTL was 1.3, 0.7, and 0.4 μg m^{-3} for SO_4^{2-}, NH_4^+, and NO_3^-, respectively. The maximum difference concentration of BC can be as high as 1.2 μg m^{-3} at 2000-2500 m between the flights F0319 and F0317 (Fig.7c). Regarding the variation in hydrocarbon species such as ACN (Fig. 7d) and ACE (Fig. 7e) in the BPTL, their maximum mean concentrations in the flight F0319 were higher than those in the profile of the flight F0317 by 0.18 and 0.9 ppb, respectively. In other words, flight F0319 had a more significant impact on the CO, OA, BC, and volatile organic compound (VOC) species such as ACN and ACE in the BPTL, which might account for the effect of BB emission transport from Indochina. The ozone concentration was lower in both flights F0317 and F0319 than in the mean profile at the elevations <2000 m (Fig. 7f). The ozone titration by NO_x in the low boundary might also play a role. However, it was approximately 5–7 ppb higher in the flight F0319 than in the flight F0317 between the elevations of 1500 and 3000 m. In their downwind area,

https://doi.org/10.5194/acp-2022-517
Preprint. Discussion started: 9 August 2022


Atmospheric Chemistry and Physics Discussions

LRT of BB emissions might increase this concentration further at the BPTL (Tang et al., 2003; Lin et al., 2014) and also discussed in section 4. By contrast, the J value [$J(O_1D)$] (Fig. 7g) was higher for flight F0317 than for F0319 in the elevation range 1000–3000 m, in line with high aerosol concentrations and associated cloud enhancement that typically lead to decreased photolysis frequencies [i.e., $J(O_1D)$] (Tang et al., 2003). Consistently, at altitudes >4000 m the presence of clouds below the aircraft led to greater J values. The concentrations of other species such as NO_y (Fig.7h) and HONO (Supplementary Fig. S2d) were also greater in flight F0317 than in flight F0319 by 0.4-1.2 ppb and 10-34 ppt, respectively, in the low boundary (<1500 m). At the BPTL, the concentration of NOy (1-2 ppb) in the flight F0319 was higher than in the flight F0317, but the difference was less than 0.6 ppb. The results from the TRACE-P campaign, which examined the Asian outflow of NO_y, also demonstrated large increases in NO_y concentrations (0.5-1 ppb) downwind from Asia. The NO_y consisted mainly of HNO_3 and peroxyacetyl nitrate (Miyazaki et al., 2003; Talbot et al., 2003).

4 Simulation results and discussion

4.1 Model performance and BB transport identification

Tables 1 and 2 and Fig. 8 plot the Pearson correlation coefficients between 5-min merged observations on board the HALO and the simulation for flights F0317 and F0319. Meteorological parameters such as potential temperature (theta), relative humidity (RH), and wind speed (WS) were all captured well by the model along the HALO flight path on the 2 days. The correlation coefficient (R) for meteorological parameters was high, ranging from 0.92 to 0.99 (Table 1). The strong correlation indicates the high representativeness of the reanalysis of meteorological data used in the simulation. Among the trace species and aerosol components, toluene (TOL), NO_x, ketones (KET), BC, OA, HONO, SO_2, and HCHO demonstrated an R of >0.5 (good

https://doi.org/10.5194/acp-2022-517
Preprint. Discussion started: 9 August 2022


Atmospheric Chemistry and Physics Discussions

correlation) and CO and O_3 showed an R of nearly 0.5 (Table 1). The simulation performance was investigated in the BL (<1000 m; Fig. 8), at 2000–4000 m altitude (Table 2 and Fig. 8) and for the whole period of both flights (Table 1 and Fig. 8; blue dot). Even in the BPTL, the simulated meteorological parameters presented a good correlation (R > 0.93), followed by KET, OA, BC and CO (R > 0.6) as well as O_3 and NO_y (R > 0.5) (Table 2). In other words, at the BPTL, the R for the simulation significantly increased for OA, BC, CO, and KET (Tables 1 and 2 and Fig. 8), which are indicators for BB being a source of pollution in the model. In contrast, SO_4^{2-}, NO_3^-, NH_4^+, SO_2, NO_2, and HCHO had better correlation in the lower part of the boundary layer, at altitudes <1000 m (see Fig. 8) than in the BPTL. We explain this by the transport of anthropogenic pollutants in the continental outflow in the lower part of the boundary layer in ECS.

The modeling results tended to overestimate the concentration of the species, with examples being CO (59 ppb), OA (0.5 μg m^{-3}), BC (0.3 μg m^{-3}) and O_3 (12.1 ppb; Table 2) in the BPTL. Because high concentrations of CO, BC and OA in BPTL are accurate indicators of BB in the model, the BB emission from the source of FINN data are probably also overestimated (Lin et al., 2014). Except for OA and BC, the correlations for other aerosol components such as NH_4^+, NO_3^-, and SO_4^{2-} were poor (0.23, 0.13, and −0.14, respectively). The poor correlation for SO_4^{2-} may result from the large uncertainty in the emission of SO_2.

Because the meteorological parameters were simulated well, the simulation discrepancies for chemical species are either caused by the emission estimation uncertainties or by inaccuracies in the simulation of chemical oxidation processes during LRT. Because CO, OA, and BC are accurate indicators of simulated BB transport from Indochina (Carmical et al., 2003), the airborne measurements on board the HALO are used as reference to evaluate the performance of the model for the flight

https://doi.org/10.5194/acp-2022-517
Preprint. Discussion started: 9 August 2022


Atmospheric Chemistry and Physics Discussions

F0319 (Fig. 9). The 5-min merged simulation of CO concentration with (blue line) and without (green line) BB was compared to that measured on board the HALO (red line); the concentration was mostly in the range of 100–200 ppb, with its peak approaching 300 ppb (at 01:50, 02:50, and 04:00 UTC) at the BPTL (Fig. 9a). In general, the simulation captured the CO variation along the flight path. However, it overestimated the observations by nearly 100 ppb for the simulation with BB at the BPTL during 01:00–02:00, 03:40–04:20, 05:00–05:40, and 06:30–07:20 UTC (Fig. 9a). Notably, the simulation difference was minor when the flight was in the lower part of the boundary layer (02:30 and 06:00 UTC) i.e. < 1000m or at elevations of >4000 m (03:00–03:30 and 04:20–05:00 UTC). The model underestimated CO concentration in the lower part of the boundary (<1000 m) (02:30 and 05:50–06:30 UTC) over the ECS. In conclusion, our model simulation overestimates BB emissions but underestimates continental CO emissions from China due to the underestimation of the emission inventory of the MICS-Asia III (Kong et al.,2020) was adopted in this study.

OA and BC are also important BB indicators and were reasonably captured by the model before 03:00 UTC when the flight was south of 28 °N at elevations of <4000 m (Fig. 9 b-c). The time series of simulated OA and BC has peak concentrations of nearly 4-5.5 μg m^{-3} and 2 μg m^{-3}, respectively, during HALO shuttle flights passing through the BPTL (2000–4000 m) around 01:50 and 02:50 UTC. When BB emission was not included in the simulation, the concentration peaks were not observed (see Fig. 9b-c, green plot). Similar to the simulated CO results, the simulated OA and BC overestimate the amounts of these species to the north of 30 °N at 04:00 UTC (Fig. 6a and 9). The model after 07:30 UTC, which was related to local emission before HALO landed over western Taiwan on 19 March 2018. In general, our model simulation captured reasonably well OA and BC with an R of 0.55 and 0.68, respectively. A minor mean bias for OA (BC) is 0.4 μg m^{-3} (0.2 μg m^{-3}) and the root mean square error (RMSE) of

https://doi.org/10.5194/acp-2022-517
Preprint. Discussion started: 9 August 2022


Atmospheric Chemistry and Physics Discussions

OA (BC) is 1.2 μg m^{-3} (0.4 μg m^{-3}) (Table 1). The R for OA (BC) reached 0.69 (0.71), with an RMSE of 1.0 μg m^{-3} (0.5 μg m^{-3}) when we calculated the BB transport layer only between 2000 and 4000 m (Table 2 and Fig. 8). In addition to OA and BC, simulated aerosol species such as SO_4^{2-}, and NH_4^+ were overestimated, whereas NO_3^- was underestimated although their concentrations were low (Table 2). Because the BPTL was mainly between altitudes of 2000 and 4000 m, the subsequent discussion focuses on the influence of the BPTL from Indochina on the downstream areas, particularly the ECS and Taiwan.

4.2 Effects of LRT BB plume from Indochina on East Asia

To investigate the regional impacts of BB plume transport from Indochina, we compared the simulation with and without BB emission for the events on 17 and 19 March 2018. The analysis of the calculations focused on the impact over SC, Taiwan and ECS. These three selected regions are SCA (in South China), TWA (covered the whole Taiwan), and ECSA (in the ECS) as shown in Figure 1a. After being emitted the BB pollutants from Indochina were then transported northward to China and subsequently northeastward. The exact flow pattern depended on the weather conditions and flow types (ridge or trough) at 700 hPa (3000 m) between 17 and 19 March 2018 (see Fig. 2). Consequently, we investigated the hourly variation in the area mean concentrations or mixing ratios of air pollutant trace constituents to assess the importance of BB emissions from Indochina on the selected downstream region e.g. the ECSA (Fig. 10), SCA, TWA and ECSA (Table 3). The contribution of CO (or others species) due to BB was estimated by detraining the difference between simulations with and without the BB emission. These differences are then expressed as a fraction in percentage shown in Figure 10 (blue line). The mean concentration of CO (red line) over the ECSA (Fig. 10a) was at its lowest (115 ppb) on 17 March 2018; it gradually increased to a peak concentration of 280 ppb on 18 March 2018 and then remained

https://doi.org/10.5194/acp-2022-517
Preprint. Discussion started: 9 August 2022


Atmospheric Chemistry and Physics Discussions

452 stable at 260 ppb on 19 March 2018. The contribution of CO from BB (blue line) ranged
453 from 19 % (<22 ppb) on 17 March 2018 to a peak of 42 % (~113 ppb) on 18 March
454 2018 and then gradually declined to 26 % on 19 March 2018 (Fig. 10a). As for OA
455 (BC), the lowest percent contribution by BB was 14-16% (<5%) between 16 and 17
456 March 2018 while the highest could be more than 30% (60%) during 18 and 19 March
457 2018 (Fig. 10b and c). The variation trend of $PM_{2.5}$ its lowest percent contribution by
458 BB was 21 % (0.42 μg m^{-3}) on 17 March 2018 (Fig. 10d), increasing to 40 % (5.6 μg
459 m^{-3}) on 18 March 2018 because the BB plume spread by the strong wind to the ECSA.
460 The variation of O_3 (Fig. 10e) depends on transport and photochemistry, which
461 involves the precursors NO_x and VOC and the photolysis frequency of NO_2, J(NO_2).
462 For the elevations between 2000–4000 m, O_3 changes are similar to those of CO, NOx
463 and KET, which were mainly contributed by the LRT BB plume and related to the
464 ozone precursor after 18 March 2018. The lowest and highest O_3 concentrations on 17
465 and 18 March 2018 were 56 and 75 ppb, respectively, of which we estimate that 5.6
466 ppb (10 %) and 34 ppb (45 %) were BB's contributions, respectively. Although the
467 mean NO_x concentration was relatively small (0.06–0.18 ppb), the BB contributed 35–
468 70 % (0.02–0.13 ppb) during 17–19 March 2018 (Supplementary Fig. S3a). The KET
469 concentration was in the range 0.4 to 2.7 ppb, with BB contributing nearly 20–26 %
470 (0.08–0.7 ppb) during 17–19 March 2018 (Supplementary Fig. S3b).
471 The area-mean OH contributed by BB increased from its lowest level (<30 %) on
472 17 March 2018 to its highest (nearly 70 %) on 19 March 2018 (Fig. 10f). HO_2 was also
473 observed to increase trend from 10 % to 40 % during daytime over the period 17–19
474 March 2018 (Supplementary Fig. S3c). The amounts of the oxidizing agent, OH, and
475 the free radical HO_2 depend on the amounts of trace gases, which produce and remove
476 these radicals, (eg. NO_x, water vapor, ozone, hydrocarbons, etc.) and the relevant
477 photolysis frequencies J(O_3→O1D), J(NO_2) etc.. Thus trace constituents from BB were

https://doi.org/10.5194/acp-2022-517
Preprint. Discussion started: 9 August 2022


Atmospheric Chemistry and Physics Discussions

478 expected to increase OH and HO_2. However, BB's contribution to photolysis
479 frequencies $J(O_3 \rightarrow O^1D)$ (Fig. 10g), $J(NO_2)$ (Supplementary Fig. S3d) etc. decreased
480 as the mean BB aerosol concentration increased over the ECS during 17–19 March
481 2018. This is because photolysis calculation results used simulated aerosol and cloud
482 formation, which increased over the ECSA (Fig. 12).

483 The NO_y, mean concentration ranged from 1.0 to 4.5 ppb, of which BB's
484 contribution was from 55 to 82 % (Supplementary Fig. S3e). Such a high contribution
485 from BB also demonstrated the effects of long-distance transport. Figure 10h indicates
486 an increasing trend of HCHO concentration from 17 to 19 March 2018. HCHO
487 formation and destruction depend on the rate of reaction of OH with HCHO precursors
488 and the rate of reaction of HCHO with OH and the photolysis frequency of HCHO. As
489 a result, HCHO production varied with OH concentration. The lowest and highest
490 concentrations of HCHO were on 17 and 19 March 2018, respectively. In summary,
491 the consistent variations in BB contributions to CO, $PM_{2.5}$, VOC, OH, NO_x, NO_y, and
492 O_3 peaked on 18 or 19 March 2018, whereas $J(O^1D)$ decreased between 17 and 19
493 March 2018.

494 Figure 11 displays the fraction in % that the long-range transported BB emission
495 contributes to the amounts of NO_x, NO_y, $PM_{2.5}$, OA, BC, OH, O_3, CO, KET, HO_2,
496 HCHO and $J(O^1D)$, over the ECSA on 17 and 19 March 2018. Except for NO_y, BB
497 contribution was generally <11 % at elevations of <1000 m over the ECSA. The scatter
498 distribution of the simulation results indicates that the effect of BB emission at
499 elevations of <1000 m (Fig. 11a) was significantly lower than that between the
500 elevations of 2000 and 4000 m (Fig. 11b). For NO_y, NO_x, $PM_{2.5}$, BC, OH, O_3, and CO,
501 the BB contribution was >30 % at the elevation of 2000–4000 m over the ECSA (Fig.
502 11b). Table 3 further summarizes the effect of BB emission on the downwind areas
503 (SCA, TWA, and the ECSA) at the <1000 m and 2000–4000 m elevations. The

https://doi.org/10.5194/acp-2022-517
Preprint. Discussion started: 9 August 2022


Atmospheric Chemistry and Physics Discussions

contribution of BB to NO_y, NO_x, $PM_{2.5}$, BC, OH, O_3 and CO was at least 30–80 % at the elevation of 2000–4000 m over the regions SCA, TWA and ECSA. In the lower boundary layer (i.e. <1000 m), the BB contribution for most species at the remote downstream areas was <20 %, except for TWA. Because of the high mountains (Lin et al. 2021) present in TWA, the BB plume passing over Taiwan was potentially transported downward through mountain–valley circulation to the lower boundary layer (Ooi et al., 2021). The influence of BB over TWA was the highest among these three downstream regions (see Table 3) as its location was directly on the transport pathway for the BB plume on the major event day (flight F0319).

Figure 12 displays the simulated cloud water difference with and without BB emission over different regions on 17 and 19 March 2018. BB aerosols are a potential source of cloud nuclei. The simulations show the impact of BB on cloud water enhancement (Fig. 12). Cloud water enhancement over SCA was associated with aerosol enhancement from the BB in the altitude range 1000–4000 m: the peak being 2-2.5 mg kg^{-1} at 2000 m on these 2 days (Fig. 12). The abundance of BB emissions transported from Indochina to SCA (Fig. 3) is expected to contribute to the high cloud water formation over SCA. Furthermore, the southerly flow (Fig. 3) that transports warm and moist air mass from the South China Sea may have favored cloud formation in flights F0317 and F0319. High cloud water related to BB can be seen in the simulations of these two days. In the remote ECSA regions, the cloud water substantially increased on 19 March 2018 (Fig. 12) compared to 17 March 2018 because of a significant difference in BB emissions transported to the ECSA between 17 and 19 March 2018 (Fig. 3). Similarly, the cloud water enhancement over Taiwan also only appeared on 19 March 2018 (Fig. 12). Furthermore, nearly no difference in the cloud water vertical distribution over the region IDCA (Fig. 1a) in Indochina was noted because in the Indochina region, spring is the dry season (Lin et al., 2009) and

https://doi.org/10.5194/acp-2022-517
Preprint. Discussion started: 9 August 2022


Atmospheric Chemistry and Physics Discussions

thus unfavorable for cloud water formation. The simulated downward short wave flux at ground surface was 1-3% reduction over the regions ECSA and SCA (supplementary Fig. S4) during 18-19 March 2018. The combination of BB aerosols enhancement and increased cloud water results in shortwave radiation reduction, implying the possibility of regional climate change in East Asia driven by BB aerosols.

5. Summary

The BB during spring in Indochina has a significant impact on the chemistry and composition of the troposphere in the surrounding regions of East Asia. During the EMeRGe campaign in Asia, atmospheric pollutants were measured on board the HALO aircraft. In this study, a minor long-range BB transport event was observed from Indochina on 17 March 2018 (flight F0317), followed by a major long-range BB transport event on 19 March 2018 (flight F0319). The impact on tropospheric trace constituent composition and the environment has been investigated.

During the major BB transport event F0319, the 1-min mean of the peak concentrations of the trace constituents CO, O3, ACE, ACN, OA and BC between the altitudes of 2000 and 4000 m over the ECS were 312.0 ppb, 79.0 ppb, 3.0 ppb, 0.6 ppb, 6.4 μg m^{-3}, 2.5 μg m^{-3} respectively. In comparison during the F0317 event CO, O3, ACE, ACN, OA and BC were 203.0 ppb, 71.0 ppb, 2.0 ppb, 0.3 ppb, 3.4 μg m^{-3}, 1.2 μg m^{-3} respectively.

When the elevation was <1000 m for both the F0317 and F0319 events, the sulfates, rather than OA, had the highest concentrations. The peak concentration could be as high as 5.1 μg m^{-3} in the low boundary for the event F0317 in the ECS. This observation is most likely explained by a continental outflow from regions having fossil fuel combustion in the lower boundary layer over the ECS.

In this study, the WRF-Chem model was employed to evaluate the BB plume

https://doi.org/10.5194/acp-2022-517
Preprint. Discussion started: 9 August 2022


Atmospheric Chemistry and Physics Discussions

556 transported from Indochina and its influence on the downstream areas including South
557 China, Taiwan, and the ECS. The contribution of the BB plume for most species in the
558 remote downstream areas was <20 % in the lower boundary layer (altitude <1000 m).
559 In comparison, the contribution of long-range transported BB plume was 30–80 %, or
560 even higher, for many of the trace constituents (NO_y, NO_x, CO, OH, O_3, BC and $PM_{2.5}$)
561 in the altitude range between 2000 and 4000 m for SC, Taiwan, and the ECS. The large
562 influence of BB over Taiwan is most probably because the BB transport passes directly
563 over Taiwan.

564 BB aerosols are potential sources of cloud nuclei. The WRF simulations estimate
565 the effect of the BB plume on cloud water formation over SC and the ECS. We observe
566 in the simulations cloud water enhancement over SC at elevations of 1000–4000 m.
567 This increase of cloud water is consistent with an increase in aerosol, caused by BB
568 emissions, transported from Indochina to SC. In remote regions of the ECS, the
569 simulated cloud water was significantly larger during the major BB event on 19 March
570 2018 than the minor BB event on 17 March 2018. The simulated decrease of the
571 photolysis frequency ($J(O^1D)$ and J (NO_2)) is attributed to the difference in aerosol
572 concentrations and associated cloud enhancement between the two events over the ECS.
573 This we explain by the significant differences in BB emissions transported to the ECS
574 between the two events.

575 Interestingly, we found the combination of increased BB aerosol concentration
576 and increased amounts of cloud water led to reductions in the amount of incoming
577 shortwave radiation at the surface over the ECS and SC. This influences tropospheric
578 chemistry and composition, regional climate, precipitation, ocean biogeochemistry,
579 agriculture and human health.

580

581 ***Data availability***

https://doi.org/10.5194/acp-2022-517
Preprint. Discussion started: 9 August 2022

Atmospheric Chemistry and Physics Discussions

582 The EMeRGe data are available at the HALO database
583 (https://doi.org/10.17616/R39Q0T, DLR, 2022) and can be accessed upon registration.
584 Modeling data can be made available upon request to the corresponding author.

585 ***Author contribution***

586 CYL conceived the idea, analyzed the data, writing and editing of the manuscript. WNC
587 and YYC run the model and analyzed the data. CKC joined the manuscript
588 discussion.CYLiu provided the MODIS data. HZ and HS provided trace gases data. EF
589 provided acetonitrile data. FO performed the ozone measurement. OOK, BAH and
590 MLP were responsible for the BC measurement. KK and JS were responsible for C-
591 ToF-MS measurements. JPB and MDAH led the EMeRGe-Asia experiment. All
592 authors have read and agree to the published version of the manuscript.

593 ***Competing interests***

594 The authors declare that they have no conflict of interest.

595 ***Acknowledgments:***

596 The accomplishment of this work has financial support from the Ministry of Science
597 and Technology, Taiwan, under grants MOST 108-2111-M-001-002, 109-2111-M-001-
598 004 and 110-2111-M-001-013. We thank to National Center for High-performance
599 Computing (NCHC) for providing computational and storage resources.
600 The HALO deployment during EMeRGe was funded by a consortium comprising the
601 German Research Foundation (DFG) Priority Program HALO-SPP 1294, the Institute
602 of Atmospheric Physics of DLR, the Max Planck Society (MPG), and the Helmholtz
603 Association. Johannes Schneider and Katharina Kaiser acknowledge funding through
604 the DFG (project no. 316589531).
605
606
607

608 **References:**

609 Ackermann, I. J., Hass, H., Memmsheimer, M., Ebel, A., Binkowski, F. S., and Shankar,
610 U.: Modal aerosol dynamics model for Europe: development and first applications,
611 Atmos. Environ., 32, 2981–2999, https://doi.org/10.1016/S1352-2310(98)00006-5,
612 1998.
613 Ahmadov, R., McKeen, S. A., Robinson, A. L., Bahreini, R., Middlebrook, A. M., de
614 Gouw, J. A., Meagher, J., Hsie, E.- Y. Edgerton, E., Shaw, S., and Trainer, M.: A
615 volatility basis set model for summertime secondary organic aerosols over the

https://doi.org/10.5194/acp-2022-517
Preprint. Discussion started: 9 August 2022

616 eastern United States in 2006, J. Geophys. Res., 117,
617 https://doi.org/10.1029/2011JD016831, 2012.
618 Andrés Hernández, M. D., Hilboll, A., Ziereis, H., Förster, E., Krüger, O. O., Kaiser,
619 K., Schneider, J., Barnaba, F., Vrekoussis, M., Schmidt, J., Huntrieser, H.,
620 Blechschmidt, A.-M., George, M., Nenakhov, V., Harlass, T., Holanda, B. A., Wolf,
621 J., Eirenschmalz, L., Krebsbach, M., Pöhlker, M. L., Kalisz Hedegaard, A. B., Mei,
622 L., Pfeilsticker, K., Liu, Y., Koppmann, R., Schlager, H., Bohn, B., Schumann, U.,
623 Richter, A., Schreiner, B., Sauer, D., Baumann, R., Mertens, M., Jöckel, P., Kilian,
624 M., Stratmann, G., Pöhlker, C., Campanelli, M., Pandolfi, M., Sicard, M., Gómez-
625 Amo, J. L., Pujadas, M., Bigge, K., Kluge, F., 770 Schwarz, A., Daskalakis, N.,
626 Walter, D., Zahn, A., Pöschl, U., Bönisch, H., Borrmann, S., Platt, U. and Burrows,
627 J. P.: Overview: On the transport and transformation of pollutants in the outflow of
628 major population centres –observational data from the EMeRGe European intensive
629 operational period in summer 2017. Atmos. Chem. Phys., 22, 5877–5924,
630 https://doi.org/10.5194/acp-22-5877-2022, 2022.
631 Carmichael, G. R., Tang,Y., Kurata, G., Uno, I., Streets, D., Woo, J.-H., Huang, H.,
632 Yienger, J., Lefer, B., Shetter R. et al.: Regional-scale chemical transport modeling
633 in support of the analysis of observations obtained during the TRACE-P experiment,
634 J. Geophys. Res., 108(D21), 8823, doi:10.1029/ 2002JD003117, 2003.
635 Chuang, M.T., Fu, J.S., Lee, C.T., Lin, N.H., Gao, Y.,Wang, S.H., Sheu, G.R., Hsiao,
636 T.C., Wang, J.L., Yen, M.C., Lin, T.H. and Thongboonchoo, N.: The simulation of
637 long-range transport of biomass burning plume and short-range transport of
638 anthropogenic pollutants to a mountain observatory in East Asia during the 7-
639 SEAS/2010 Dongsha Experiment. Aerosol Air Qual. Res. 16: 2933–2949, 2016.
640 Chi K H., C. Y. Lin, C.F.Ouyang, J.Lin Lin, N.H. Lin, G.R. Sheu, C. T. Lee: PCDD/F
641 Measurement at a High-altitude Station in Central Taiwan: Evaluation of Long-range
642 Transport of PCDD/Fs during the Southeast Asia Biomass Burning Event,
643 *Environmental Science & Technology,44,2954-2960,* DOI: 10.1021/es1000984
644 https://doi.org/10.1021/es1000984, 2010.
645 Ding K., Huang X., Ding A., Wang M., Su H., et al.: Aerosol-boundary-layer-monsoon
646 interactions amplify semi-direct effect of biomass smoke on low cloud formation in
647 Southeast Asia., Nature Communications, 12:6416, 2021.
648 Fu, J. S., Hsu, N. C., Gao, Y., Huang, K., Li, C., Lin, N.-H., and Tsay, S.-C.: Evaluating
649 the influences of biomass burning during 2006 BASE-ASIA: a regional chemical
650 transport modeling, Atmos. Chem. Phys., 12, 3837–3855,
651 https://doi.org/10.5194/acp-12-3837-2012, 2012.
652 Galanter, M., Levy, H., Carmichael, G. R.: Impacts of biomass burning on tropospheric
653 CO, NOx, and O3, J. Geophys. Res. Atmos., 105, 6633-6653, 2000.

https://doi.org/10.5194/acp-2022-517
Preprint. Discussion started: 9 August 2022

Atmospheric Chemistry and Physics Discussions

654 Giglio, L., Randerson, J.T., Werf, G.R.V.D.: Analysis of daily, monthly, and annual
655 burned area using the fourth-generation global fire emissions database (GFED4). J.
656 Geophys. Res. Biogeosci. 118 (1), 317–328., 2013.
657 Grell, G. A., Peckham, S. E., Schmitz, R., McKeen, S. A., Frost, G., Skamarock, W. C.,
658 and Eder, B.: Fully coupled "online" chemistry within the WRF model, Atmos.
659 Environ., 39, 6957–6975, https://doi.org/10.1016/j.atmosenv.2005.04.027, 2005.
660 Heald, C. L., Jacob D.J., Fiore, A.M., Emmons, L. K., et al.: Asian outflow and trans-
661 Pacific transport of carbon monoxide and ozone pollution: An integrated satellite,
662 aircraft, and model perspective, J. Geophys. Res., 108(D24), 4804,
663 doi:10.1029/2003JD003507, 2003.
664 Hong, S., Lakshmi V., Small, E.E., Chen, F., Tewari, M., Manning, K.W.: Effects of
665 vegetation and soil moisture on the simulated land surface processes from the
666 coupled WRF/Noah model. J Geophys Res 114(D18), D18118, 2009.
667 Huang, K., Fu, J. S., Hsu, N.C., Gao, Y., Dong, X., Tsay, S. C., Lam, Y. F.: Impact
668 assessment of biomass burning on air quality in Southeast and East Asia during
669 BASE-ASIA, Atmospheric Environment, 78, 291e302, 2013.
670 Jacob, D.J., Crawford, J. H. Kleb, M. M.,Connors, V. S, Bendura, R. J., Raper, J. L.,
671 Sachse,G. W., Gille, J. C., Emmons, L., Heald, C. L.: The transport and chemical
672 evolution over the pacific (trace-P) aircraft mission: design, execution, and first
673 results. J. Geophys. Res. Atmos. 108 (D20), 2003.
674 Janjic, Z.I.: The step-mountain eta coordinate model: further developments of the
675 convection,viscous layer, and turbulence closure schemes, Mon.Wea. Rev., 122,
676 927–945, 1994.
677 Kong L., Tang X., Zhu J., Wang Z., Fu J.S., Wang X., et al.: Evaluation and uncertainty
678 investigation of the NO2, CO and NH3 modeling over China under the framework
679 of MICS-Asia III. Atmos. Chem. Phys., 20, 181–202, 2020.
680 https://doi.org/10.5194/acp-20-181-2020
681 Li, J., Nagashima,T., Kong, L., Ge, B., Yamaji, K., Fu, J. S., Wang X., Fan, Q., Itahashi ,
682 S.,et al.: Model evaluation and inter-comparison of surface-level ozone and relevant
683 species in East Asia in the context of MICS-ASIA phase III Part I: overview. Atmos.
684 Chem. Phys., 19, 12993–13015, https://doi.org/10.5194/acp-19-12993-2019, 2019.
685 Lin, C.Y., Hsu, H.M., Lee, Y.H., Kuo, C. H., Sheng, Y.F., Chu, D. A.: A new transport
686 mechanism of biomass burning from Indochina as identified by modeling studies.,
687 *Atmos. Chem. Phys*., 9, 7901-7911. https://doi.org/10.5194/acp-9-7901-2009 ,2009.
688 Lin, C. Y., Chou, C.C.K, Wang, Z., Lung, S.C., Lee, C. T., Yuan, C.S., Chen, W. N.,
689 Chang, S. Y., Hsu, S. C., Chen, W. C., Liu, Shaw. C.: Impact of different transport
690 mechanisms of Asian dust and anthropogenic pollutants to Taiwan. Atmospheric
691 Environment, 60,403-418, http://dx.doi.org/10.1016/j.atmosenv.2012.06.049, 2012.

https://doi.org/10.5194/acp-2022-517
Preprint. Discussion started: 9 August 2022


Atmospheric Chemistry and Physics Discussions

692 Lin, C. Y., Zhao, Liu, C. X, Lin, N. H., Chen, W. N.: Modeling of long-range transport
693 of Southeast Asia biomass burning pollutants to Taiwan and their radiative forcing
694 over East Asia, *Tellus B, 66, 1-17. 23733.*
695 *http://dx.doi.org/10.3402/tellusb.v66.23733, 2014.*
696 Lin, C.Y., Sheng, Y. F., Chen, W. C., Chou, C.C. K., Chien, Y. Y., Chen, W. M.: Air
697 quality deterioration episode associated with typhoon over the complex topographic
698 environment in central Taiwan. Atmos. Chem. Phys., 21, 16839-16910.
699 https://doi.org/10.5194/acp-21-16893-2021, 2021.
700 Lin, N.H., Tsay, S.C., Reid, J. S.,Yen, M.C., Sheu, G. R.,Wang, S.H., Chi, K.H.,et al. :
701 An overview of regional experiments on biomass burning aerosols and related
702 pollutants in Southeast Asia: From BASE-ASIA and Dongsha Experiment to 7-
703 SEAS. Atmos. Environ. 78: 1–19, 2012.
704 Marvin, M. R., Palmer P. I., Latter, B. G., Siddans, R., Kerridge, B.J., Latif, M. T., Khan,
705 M. F.: Photochemical environment over Southeast Asia primed for hazardous ozone
706 levels with influx of nitrogen oxides from seasonal biomass burning. Atmos. Chem.
707 Phys., 21, 1917–1935. https://doi.org/10.5194/acp-21-1917-2021, 2021.
708 Miyazaki Y., Kondo Y., Koike M., Fuelberg H. E., Kiley C. M., Kita K., Takegawa N.,
709 Sachse G. W., Flocke F., Weinheimer A. J., Singh H. B., Eisele F. L., Zondlo M.,
710 Talbot R. W., Sandholm S. T., Avery M. A., Blake D. R.: Synoptic-scale transport of
711 reactive nitrogen over the western Pacific in spring, J. Geophys. Res.,
712 108(D20),8788, doi:10.1029/2002JD003248., 2003.
713 Morrison H., Curry, J.A., Khvorostyanov,V.I.: A new double-moment microphysics
714 parameterization for application in cloud and climate model. PartI: Description.
715 *Journal of the Atmospheric Sciences.*, 62, 1665-1676, 2005.
716 Palmer, P. I., Jacob, D. J., Jones, D. B. A., Heald, C. L., Yantosca, R. M., Logan, J. A.,
717 Sachse, G. W. and Streets, D. G.: Inverting for emissions of carbon monoxide from
718 Asia using aircraft observations over the western Pacific, *J. Geophys. Res*., 108(D21),
719 8828, doi:10.1029/2003JD003397, 2003.
720 Pimonsree, S., Vongruang, P., Sumitsawan, S.: Modified biomass burning emission in
721 modeling system with fire radiative power: Simulation of particulate matter in
722 Mainland Southeast Asia during smog episode. *Atmospheric Pollution Research*, 9,
723 133-145. http://dx.doi.org/10.1016/j.apr.2017.08.002, 2018.
724 Ramanathan, V., Ramana, M. V., Roberts, G., Kim, D., Corrigan, C., Chung, C., and
725 Winker, D.: Warming trends in Asia amplified by brown cloud solar absorption.
726 *Nature*, 448, 575-U575, 2007.
727 Reid, J. S., Hyer, E. J., Johnson, R. S., Holben, B. N., Yokelson, R. J., Zhang, J., et al. :
728 Observing and understanding the Southeast Asian aeroslo system by remote sensing:
729 An initial review and analysis for the Seven Southeast Asian Studies (7SEAS)

https://doi.org/10.5194/acp-2022-517
Preprint. Discussion started: 9 August 2022

Atmospheric Chemistry and Physics Discussions

program, Atmospheric Research, 122, 403-468, 2013.

Shi, Y., Yamaguchi, Y.: A high-resolution and multi-year emissions inventory for biomass burning in Southeast Asia during 2001-2010. Atmospheric Environment, 98, 8-16, http://dx.doi.org/10.1016/j.atmosenv.2014.08.050, 2014.

Stein, A. F., R. R. Draxler, G. D. Rolph, B. J. B. Stunder, M. D. Cohen, and F. Ngan. : NOAA's HYSPLIT Atmospheric Transport and Dispersion Modeling System, Bulletin of the American Meteorological Society 96, 12 (2015): 2059-2077, https://doi.org/10.1175/BAMS-D-14-00110.1, 2021.

Stockwell, W. R., Middleton, P., Chang, J. S., and Tang, X.: The second generation regional acid deposition model chemical mechanism for regional air quality modeling, J. Geophys. Res., 95, 16343–16367, 1990.

Talbot, R., Dibb, J., Scheuer E., Seid G., Russo R., Sandholm S., Tan D., Singh H., Blake D., Blake N., Atlas E., Sachse G., Jordan C., Avery M., 2003: Reactive nitrogen in Asian continental outflow over the western Pacific: Results from the NASA Transport and Chemical Evolution over the Pacific (TRACE-P) airborne mission. J. Geophys. Res., 108 (D20), doi:10.1029/2002JD003110, 2003.

Tang, Y., Carmichael, G. R., Woo, Jung-Hun, Thongboonchoo N., Kurata, G., Uno,I., Streets D. G., et al.: Influences of biomass burning during the Transport and Chemical Evolution Over the Pacific (TRACE-P) experiment identified by the regional chemical transport model, J. Geophys. Res., 108(D21), 8824, 2003.

Wiedinmyer, C., Akagi, S. K., Yokelson, R. J., Emmons, L. K., Al-Saadi, J.A., Orlando, J. J., and Soja, A. J.: The Fire INventory from NCAR (FINN): a high resolution global model to estimate the emissions from open burning, *Geosci. Model Dev*., **4**, 625-641, doi:10.5194/gmd-4-625-2011, 2011.

Xu, R., Tie, X., Li, G., Zhao, S., Cao, J., Feng T., Long X., Effect of biomass burning on black carbon (BC) in South Asia and Tibetan Plateau: The analysis of WRF-Chem modeling. Science of the Total Environment，645,901-912., 2018.

Yadav, I. C., Devi, N. L., Li, J., Syed, J. H., Zhang, G., Watanabe, H.: Biomass burning in Indo-China peninsula and its impacts on regional air quality and global climate change-a review. Environmental Pollution, 227, 414-427, 2017.

Zhao, C., Liu, X., Leung, L. R. and Hagos, S.: Radiative impact of mineral dust on monsoon precipitation variability over West Africa. *Atmos. Chem. Phys.*, **11**, 1879-1893, 2011.

https://doi.org/10.5194/acp-2022-517
Preprint. Discussion started: 9 August 2022

Atmospheric Chemistry and Physics Discussions

768
769
770
771
772

773 Table 1 Observed and simulated mean values for bias (BIAS), root mean square error
774 (RMSE), and correlation coefficients (R) for EMeRGe HALO flights on 17 and 19
775 March 2018. KET*: the observed Acetone is applied to compare with simulated ketones
776 (KET).

	OBS_ave	SIM_ave	BIAS	RMSE	R
THETA(K)	304.8	304.2	-0.6	1.1	0.99
WS(m/s)	9.1	8.5	-0.6	2.0	0.94
RH(%)	63.6	63.0	-0.6	10.6	0.92
OA(μg/m^3)	1.2	1.5	0.4	1.2	0.55
BC(μg/m^3)	0.4	0.5	0.2	0.4	0.68
SO_4^{2-}(μg/m^3)	1.1	2.5	1.4	2.2	0.37
NO_3^-(μg/m^3)	0.2	0.6	0.5	2.1	0.31
NH_4^+(μg/m^3)	0.4	0.7	0.3	1.1	0.49
CO(ppb)	170.8	188.9	18.1	69.6	0.46
SO_2(ppb)	0.2	0.9	0.7	1.3	0.52
O_3(ppb)	59.7	63.2	3.5	14.1	0.42
NO_x(ppb)	0.2	0.2	0.0	0.2	0.74
NO_y(ppb)	1.2	2.8	1.5	2.5	0.04
KET*(ppb)	1.4	1.5	0.1	0.9	0.59
TOL(ppb)	0.1	0.1	0.0	0.1	0.76
XYL(ppb)	0.1	0.0	0.0	0.1	0.38
HCHO(ppb)	0.1	0.7	0.6	0.7	0.50
HONO(ppt)	10.5	1.0	-9.4	15.4	0.55

777

https://doi.org/10.5194/acp-2022-517
Preprint. Discussion started: 9 August 2022

Atmospheric Chemistry and Physics Discussions

778 Table 2 Observed and simulated mean values at an elevation between 2 km and 4 km
779 for bias (BIAS), root mean square error (RMSE), and correlation coefficients (R) during
780 EMeRGe HALO flights on 17 and 19 March 2018. KET*: the observed Acetone is
781 applied to compare with simulated ketones (KET).

	OBS_ave	SIM_ave	BIAS	RMSE	R
THETA(K)	307.5	306.7	-0.8	0.9	0.98
WS(m/s)	8.2	7.9	-0.3	1.7	0.93
RH(%)	55.8	56.1	0.4	7.6	0.96
OA(μg/m^3)	1.3	1.8	0.5	1.0	0.69
BC(μg/m^3)	0.4	0.7	0.3	0.5	0.71
SO_4^{2-}(μg/m^3)	0.8	2.6	1.8	2.3	-0.14
NO_3^-(μg/m^3)	0.1	0.1	-0.1	0.4	0.13
NH_4^+(μg/m^3)	0.4	0.4	0.1	0.3	0.23
CO(ppb)	164.4	223.4	59.0	80.3	0.60
SO_2(ppb)	0.0	1.0	1.0	1.2	-0.03
O_3(ppb)	60.1	72.2	12.1	14.5	0.54
NO_x(ppb)	0.1	0.2	0.0	0.1	0.54
NO_y(ppb)	1.0	3.8	2.8	3.3	0.53
KET*(ppb)	1.5	1.9	0.4	0.9	0.71
TOL(ppb)	0.1	0.0	0.0	0.1	0.13
XYL(ppb)	0.0	0.0	0.0	0.0	-0.17
HCHO(ppb)	0.1	0.7	0.6	0.8	0.23
HONO(ppt)	6.0	0.6	-5.4	7.2	0.24

782
783
784
785
786
787
788
789
790
791
792
793
794
795
796
797
798
799
800
801

https://doi.org/10.5194/acp-2022-517
Preprint. Discussion started: 9 August 2022

Atmospheric Chemistry and Physics Discussions

802 Table 3: Simulated biomass burning contribution (with and without BB emission in
803 Indochina) in percentage (%) on 17 and 19 March, 2018 for different regions: SCA,
804 TWA, ECSA as shown in Figure 1a
805

	SCA		TWA		ECSA	
Average	< 1KM	2-4KM	< 1KM	2-4KM	< 1KM	2-4KM
NO_y	14.9	72.9	44.8	83.2	18.9	71.5
NO_x	-1.4	58.1	3.7	70.8	2.1	51.2
$PM_{2.5}$	5.8	44.6	14.7	56.4	7.2	31.9
OA	4.4	37.2	6.7	47.6	4.6	24.6
BC	6.9	74.4	14.0	81.0	6.1	42.4
OH	14.3	43.6	24.7	66.6	10.0	48.1
O3	18.8	33.7	23.5	38.5	9.4	31.0
CO	9.8	31.4	21.7	37.8	11.1	32.0
KET	6.0	17.0	9.0	26.8	7.0	24.5
HCHO	-3.5	10.2	-3.8	20.7	-4.0	10.3
HO_2	9.0	4.5	15.4	35.5	6.4	24.9
$J(O^1D)$	-3.0	-1.7	-1.1	0.4	-1.6	-1.1

806
807
808
809
810
811
812
813

https://doi.org/10.5194/acp-2022-517
Preprint. Discussion started: 9 August 2022

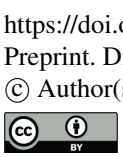

Atmospheric Chemistry and Physics Discussions

(a)

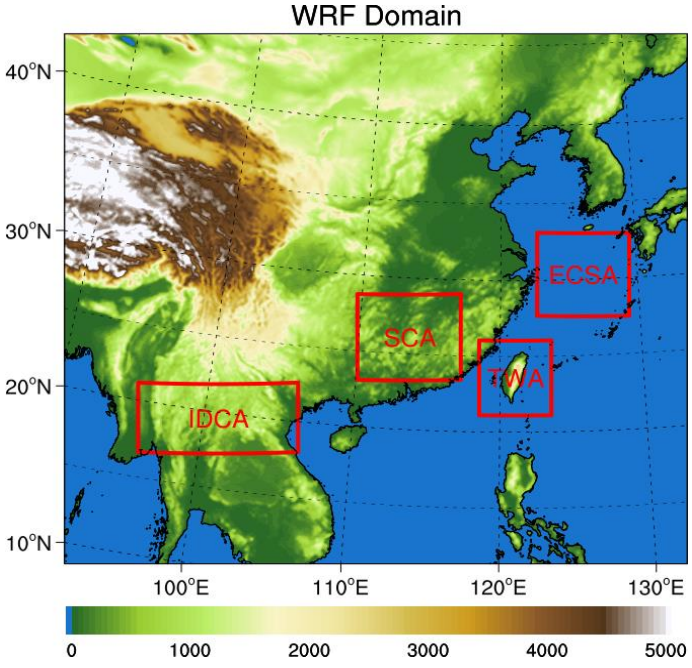

(b)

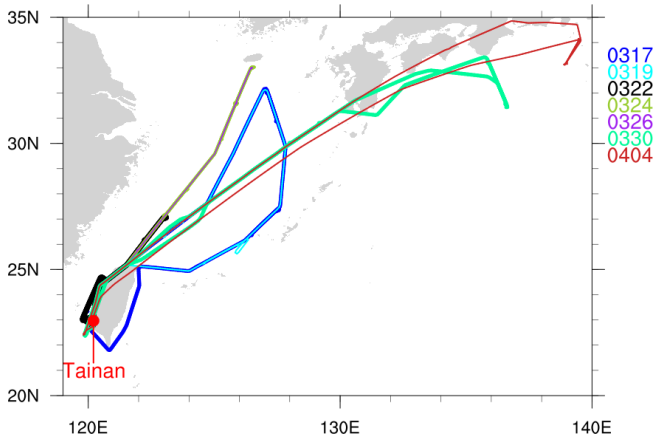

Figure 1 (a) Configuration of Weather Research and Forecasting model domain, topography, and location of proposed study areas in East Asia, namely IDCA (Indochina area), SCA (southern China area), TWA (Taiwan area) and ECSA (East China Sea area, respectively. (b) The HALO flights on 17, 19, 22, 24, 26, 30 March, and 04 April during EMeRGe Asia campaign. Different colors indicated different flights over East Asia. Maps and plots were produced using NCAR Command Language (NCL) version 6.6.2.

https://doi.org/10.5194/acp-2022-517
Preprint. Discussion started: 9 August 2022

Atmospheric Chemistry and Physics Discussions

852 (a) (b)

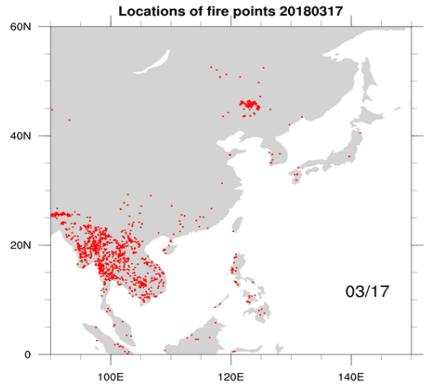

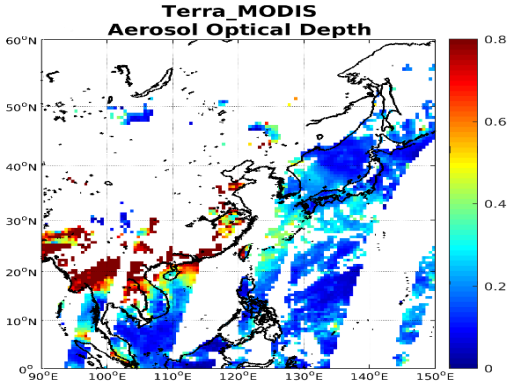

853

854

855 (c) (d)

856

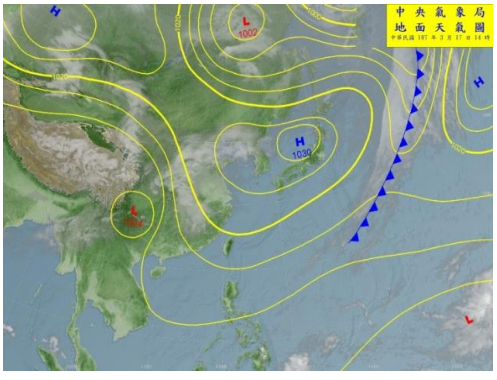

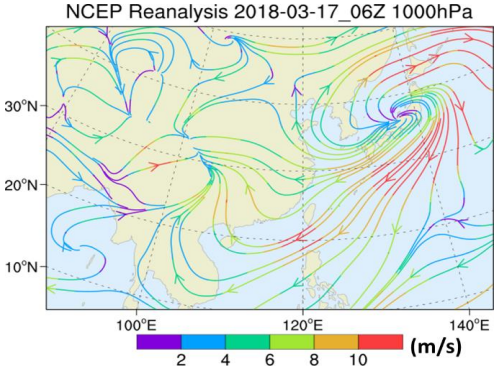

857

858 Fig.2 (a) MODIS fire hot spots on 17 March 2018 (source: https://modis-
859 fire.umd.edu/guides.html) and (b) Composited Aerosol Optical Depth (AOD) from
860 MODIS onboard NASA Terra satellite. The Collection 6.1 AOD is downloaded from
861 NASA Earth Data website (https://www.earthdata.nasa.gov/learn/find-data), and
862 composted for 0110, 0115, 0120, 0125, 0130, 0250, 0255, 0300, 0305, 0310, 0430,
863 0435, 0440, 0445, 0610, 0615, 0620, 0745 and 0750UTC data granules on 17 March
864 2018. (c) weather Chart at 06:00 UTC on 17 March 2018 (d) 1000 hPa streamlines at
865 06:00 UTC, 17 March 2018 (e) and (f) same as (c) and (d) but on 19 March 2018 ;(g)
866 700 hPa streamlines at 06:00 UTC, on 17 March 2018 (h) 700 hPa geopotential height
867 at 06:00 UTC, on 17 March 2018; (i) and (j) same as (g) and (h) but on 19 March
868 2018.

869 Near-surface weather charts and satellite images were provided by Central Weather
870 Bureau (CWB) Taiwan. The near-surface and 700 hPa streamlines and geopotential

https://doi.org/10.5194/acp-2022-517
Preprint. Discussion started: 9 August 2022

Atmospheric Chemistry and Physics Discussions

height were deduced from NCEP Reanalysis data. Maps and plots were produced using NCAR Command Language (NCL) version 6.6.2.

(e) (f)

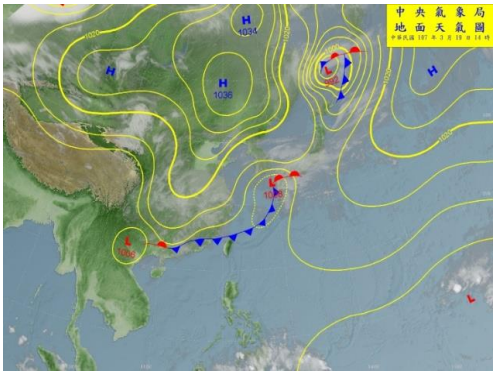

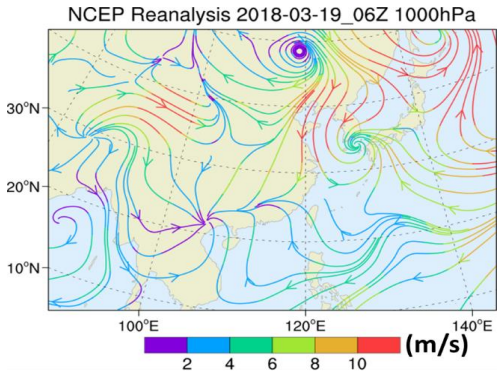

(g) (h)

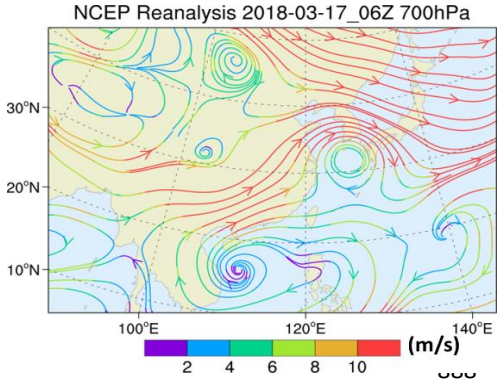

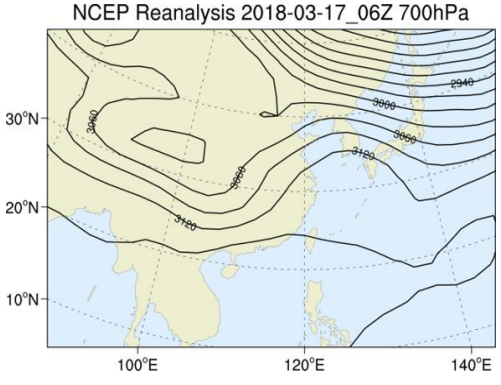

Figure 2 e-h continued

(i) (j)

https://doi.org/10.5194/acp-2022-517
Preprint. Discussion started: 9 August 2022

Atmospheric Chemistry and Physics Discussions

899
900

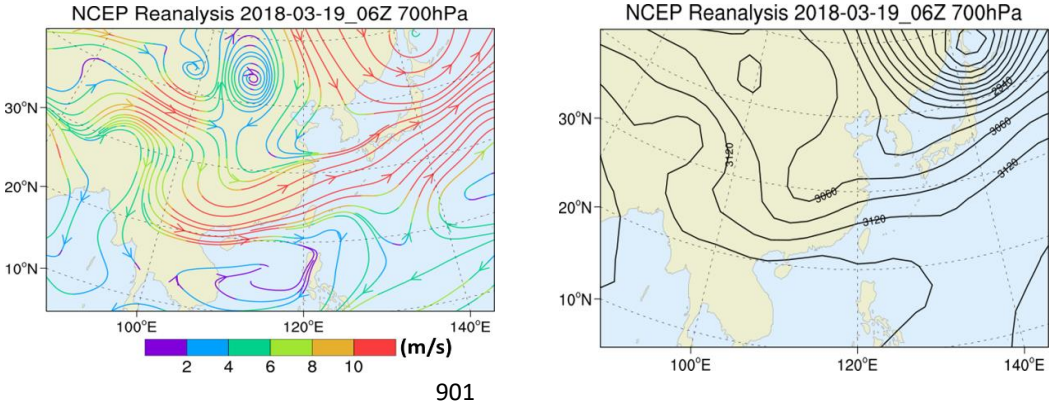

901
902
903
904
905
906
907
908
909
910
911
912
913
914
915 Fig. 2 i-j continued
916
917
918
919
920
921
922
923
924
925
926

https://doi.org/10.5194/acp-2022-517
Preprint. Discussion started: 9 August 2022

Atmospheric Chemistry and Physics Discussions

927 (a) (b)

928

929

930 (c) (d)

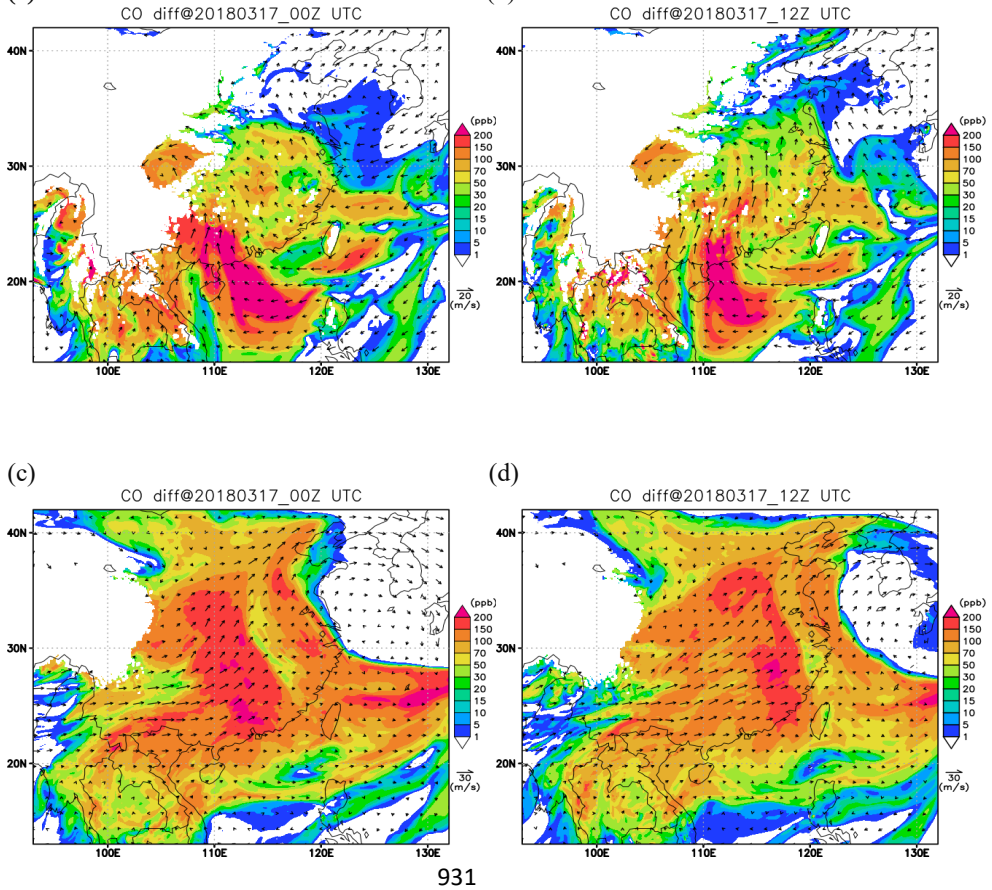

931

932

933

934 Fig 3 a-d : Simulated wind field (m s^{-1}) distribution and concentration (unit: ppb)
935 difference with and without BB emission for CO on 17 March, 2018 at 00:00 UTC (a,
936 c) and 12:00 UTC (b, d) for 1km altitude (a, b) and 3km altitude (c, d). (unit:ppb)

937

938

https://doi.org/10.5194/acp-2022-517
Preprint. Discussion started: 9 August 2022

Atmospheric Chemistry and Physics Discussions

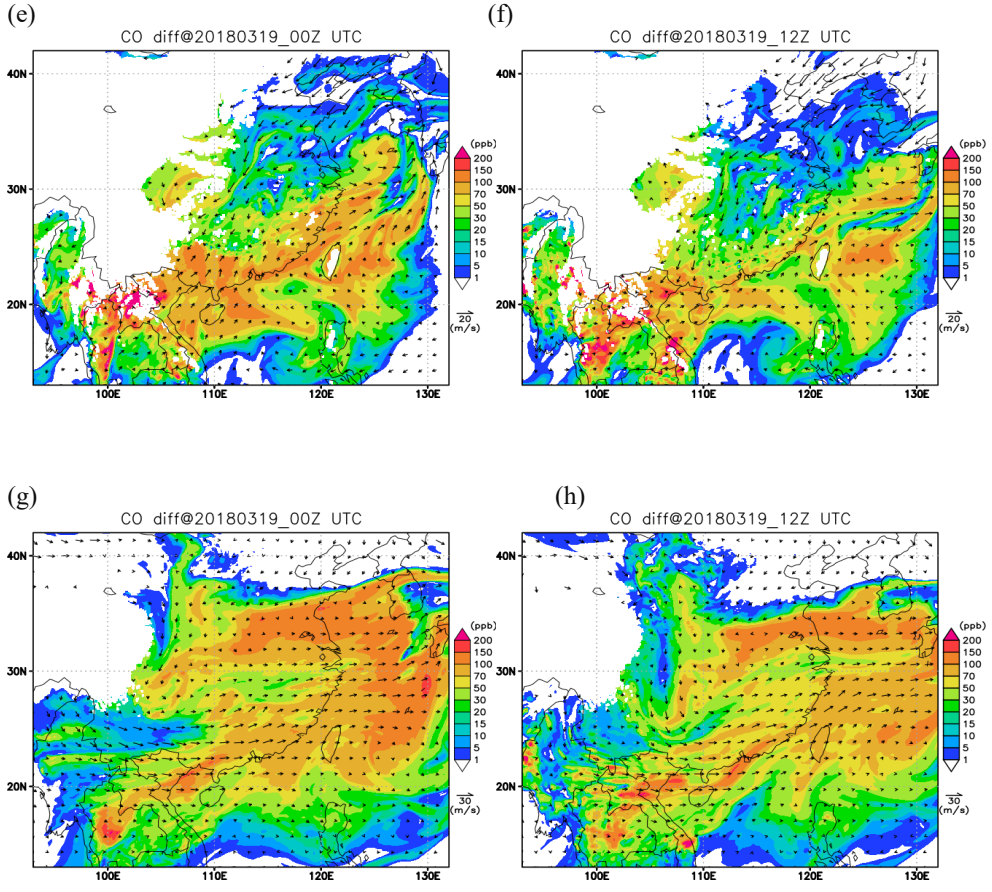

Fig 3 e-h: Simulated wind field (m s^{-1}) and concentration (unit: ppb) difference with and without BB emission for CO on 19 March, 2018 at 00:00 UTC (e, g) and 12:00 UTC (f, h) for 1km altitude (e, f) and 3km altitude (g, h).

https://doi.org/10.5194/acp-2022-517
Preprint. Discussion started: 9 August 2022

Atmospheric Chemistry and Physics Discussions

(a)

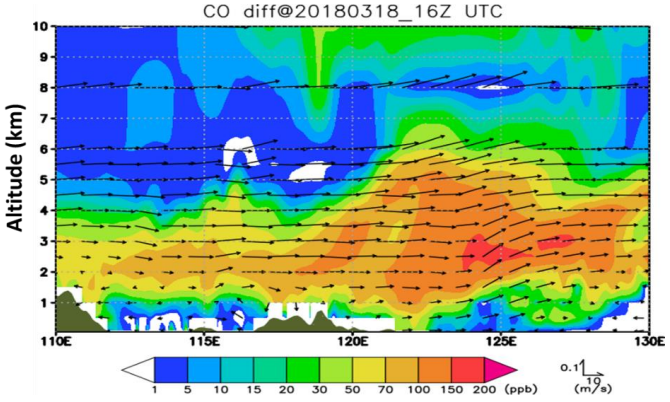

(b)

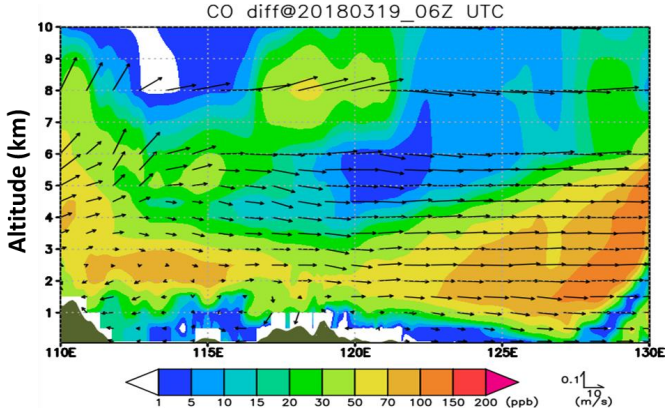

Fig. 4 Simulated wind field (m s^{-1}) distribution and the concentration (ppb) difference between with and without BB emission for CO at cross-section 30 °N (a) 16:00 UTC 18 March 2018 (b) 06:00 UTC, 19 March 2018. Wind vectors represent along section winds, with scales shown at the down-right corner of plot (unit: m s^{-1})

https://doi.org/10.5194/acp-2022-517
Preprint. Discussion started: 9 August 2022

Atmospheric Chemistry and Physics Discussions

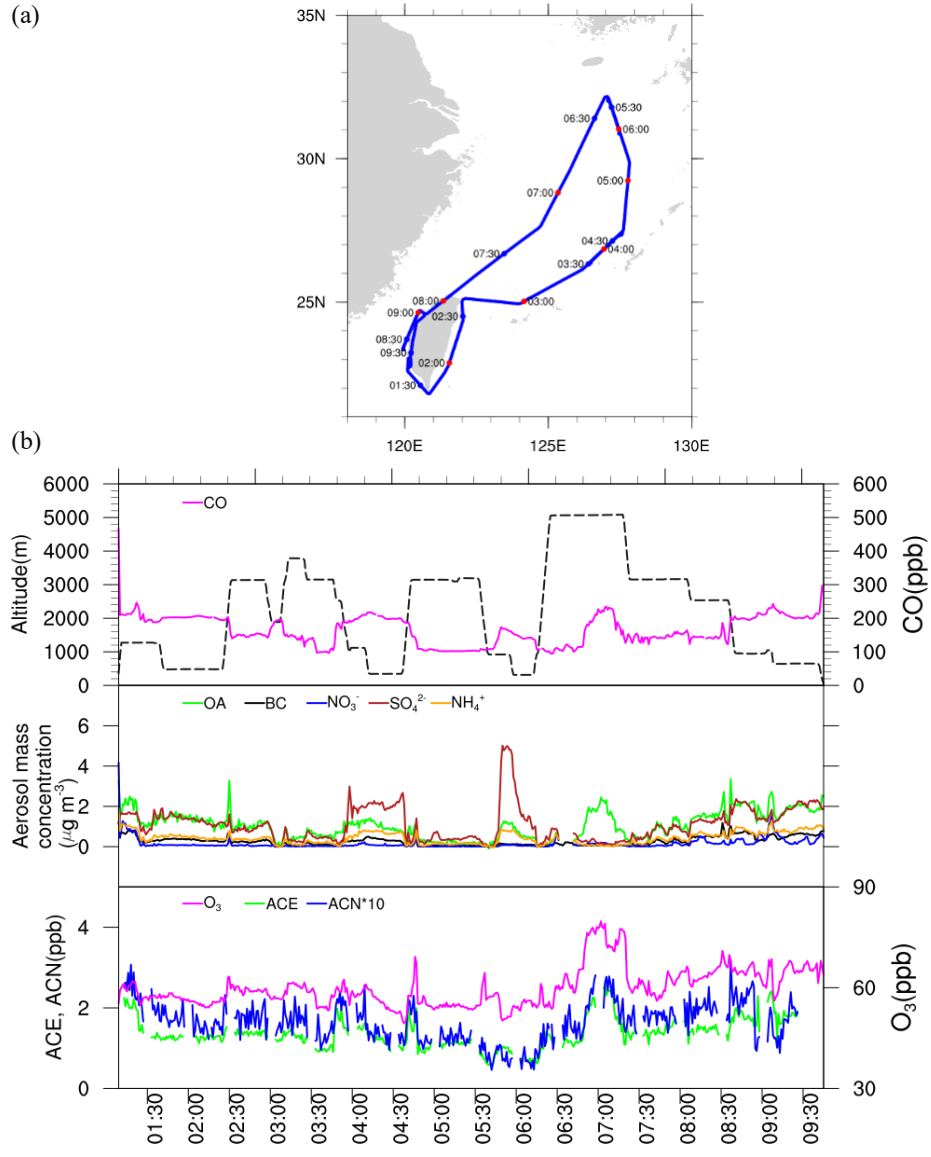

Fig. 5 (a) The HALO flight and detailed locations on 17 March 2018. (b) Flight altitude and 1-min mean of observed concentrations for CO (upper), Organic aerosol (OA), BC aerosol (BC), SO_4^{2-}, NO_3^-, NH_4^+ (middle), O_3, acetone (ACE) and acetonitrile (ACN) (bottom) on 17 March. (c) The observed SO_4^{2-} mass concentration by HALO along with height-latitude variations on 17 March 2018 (d) The observed OA mass concentration by HALO along with height-latitude variations on 17 March 2018 (e) Result of the HYSPLIT model backward trajectory analysis started at the location of the HALO flight path at 02:00, 04:00, 06:00, 09:00 UTC on 17 March 2018.

https://doi.org/10.5194/acp-2022-517
Preprint. Discussion started: 9 August 2022

Atmospheric Chemistry and Physics Discussions

(c)

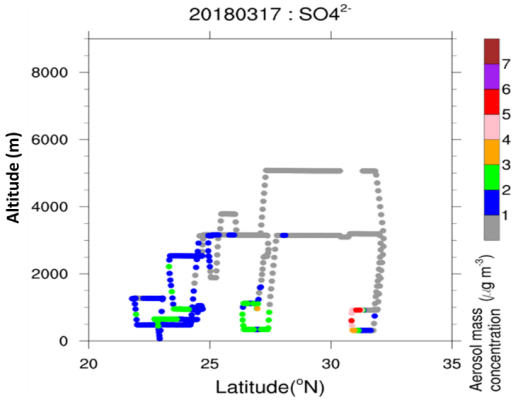

(d)

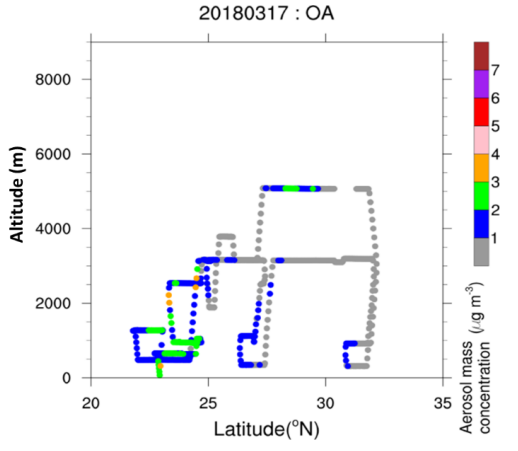

(e)

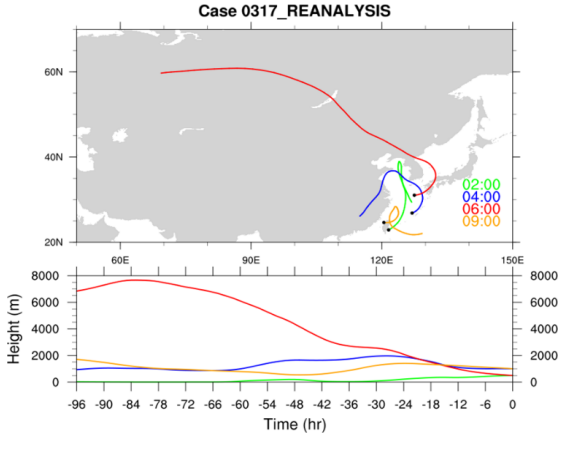

Figure 5 c-e

https://doi.org/10.5194/acp-2022-517
Preprint. Discussion started: 9 August 2022

Atmospheric Chemistry and Physics Discussions

(a)

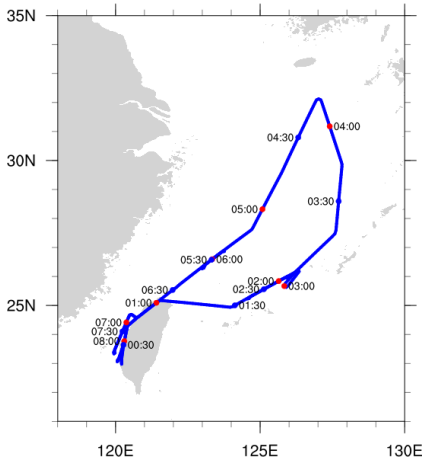

(b)

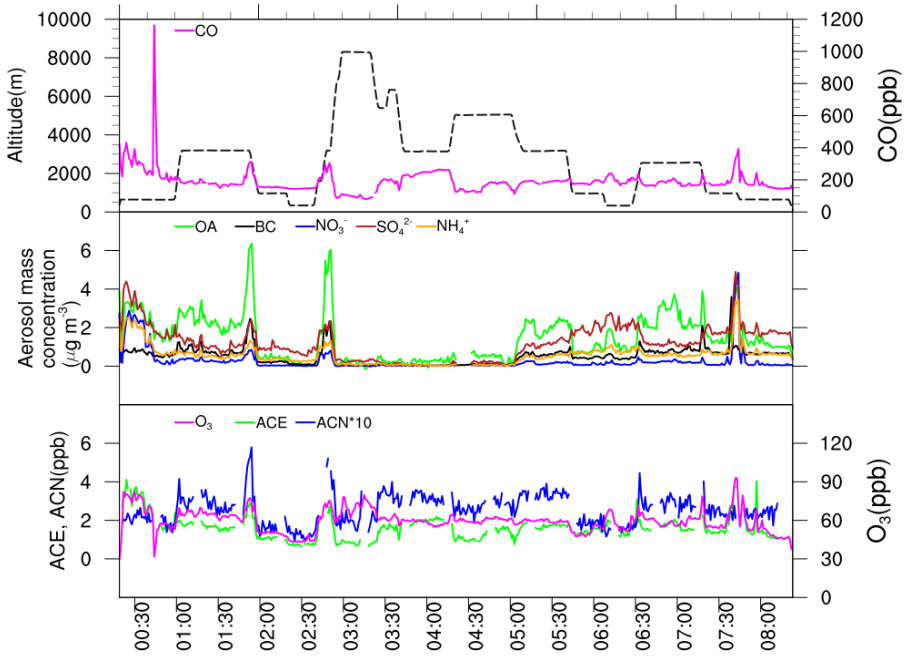

Figure 6 (a) The HALO flight and detailed locations on 19 March. (b) Flight altitude and 1-min mean of observed concentrations for CO (upper), Organic aerosol (OA), BC aerosol (BC), SO_4^{2-}, NO_3^-, NH_4^+ (middle), O3, acetone (ACE) and Acetonitrile (ACN) (bottom) on 19 March 2018. (c) The observed SO_4^{2-} mass concentration by HALO along with height-latitude variations on 19 March 2018 (d) The observed OA mass concentration by HALO along with height-latitude variations on 19 March 2018 (e) Result of the HYSPLIT model backward trajectory analysis started at the location of the HALO flight path at 02:00, 04:00, 05:00, 07:00 UTC on 19 March 2018.

https://doi.org/10.5194/acp-2022-517
Preprint. Discussion started: 9 August 2022

Atmospheric Chemistry and Physics Discussions

(c)

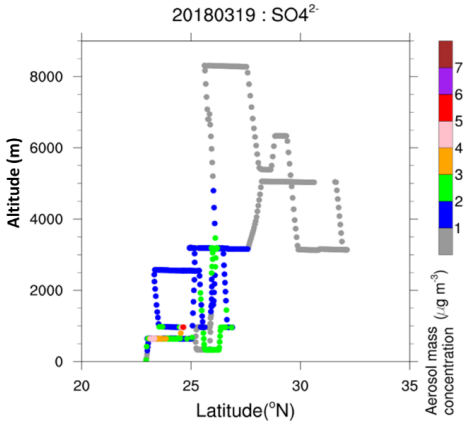

(d)

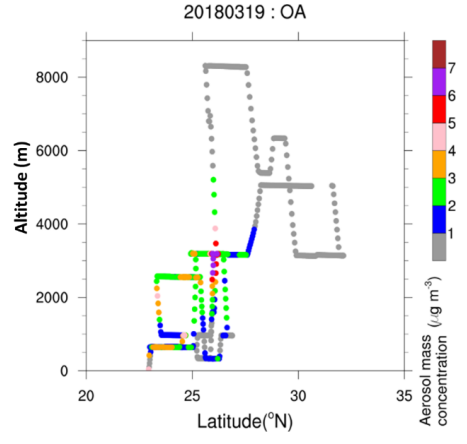

(e)

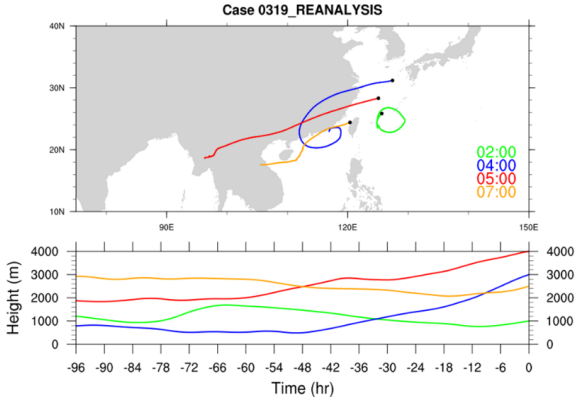

Figure 6 c-e

https://doi.org/10.5194/acp-2022-517
Preprint. Discussion started: 9 August 2022

Atmospheric Chemistry and Physics Discussions

1099 (a) (b)

1100

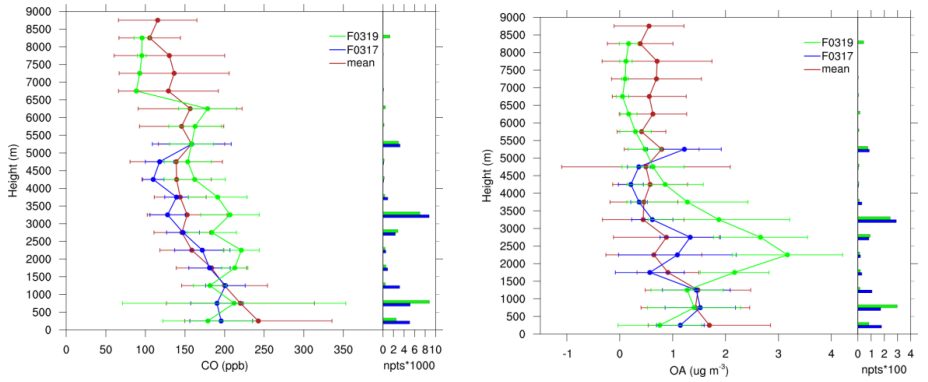

1101

1102 (c) (d)

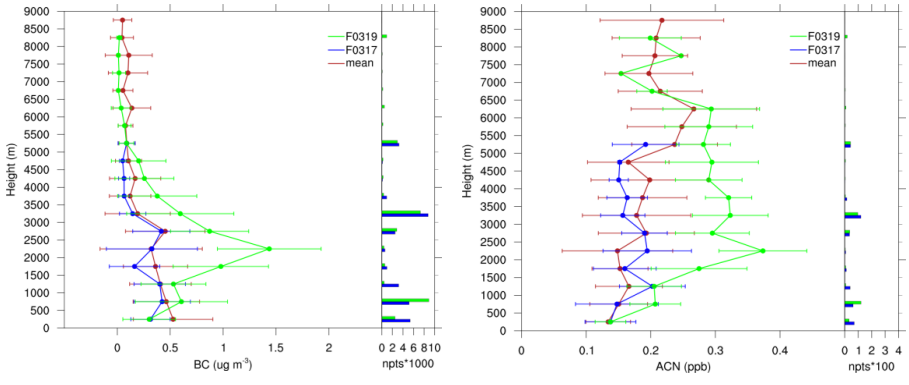

1103

1104

1105

1106

1107 Fig.7 Observed vertical distribution calculated as 1-min mean and 500 m interval with
1108 one standard deviation of the concentrations for the mean profiles (red) (including 17,
1109 19, 22, 24, 26, 30 March, and 04 April 2018) and flights on 17 (blue) and 19 (green)
1110 March 2018. (a) CO (b) OA (c) BC (d) Acetonitrile (ACN) (e) Acetone (ACE) (f) O_3
1111 (g) J (O^1D) (h) NO_y. The number of data points is shown in the right panel.

1112

1113

https://doi.org/10.5194/acp-2022-517
Preprint. Discussion started: 9 August 2022

Atmospheric Chemistry and Physics Discussions

(e) (f)

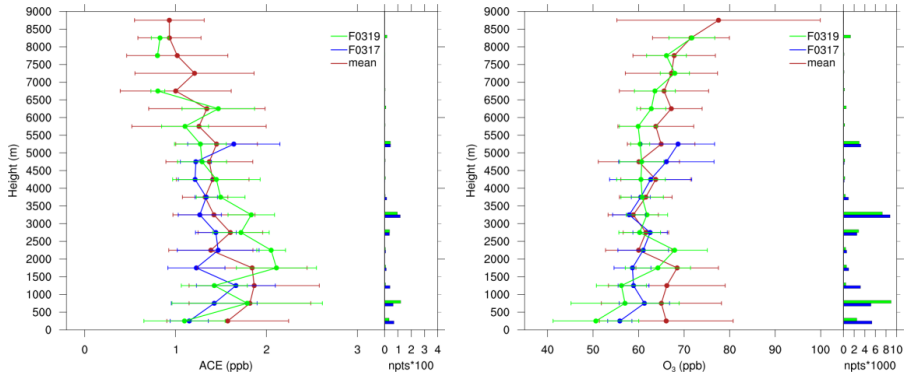

(g) (h)

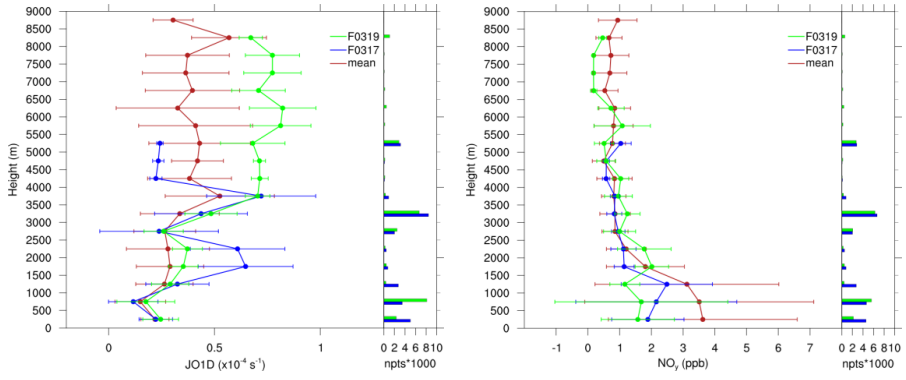

Figure 7 continued

https://doi.org/10.5194/acp-2022-517
Preprint. Discussion started: 9 August 2022

Atmospheric Chemistry and Physics Discussions

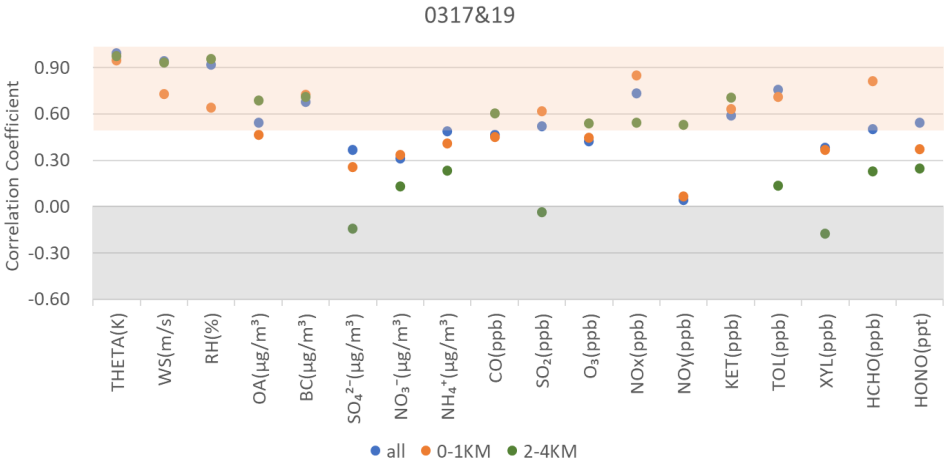

Fig. 8 Correlation Coefficient (R) between observation and simulation along with the HALO flights at the elevations 0-1 km, 2-4 km, and the whole track (all) on 17 and 19 March 2018.

https://doi.org/10.5194/acp-2022-517
Preprint. Discussion started: 9 August 2022

Atmospheric Chemistry and Physics Discussions

(a)

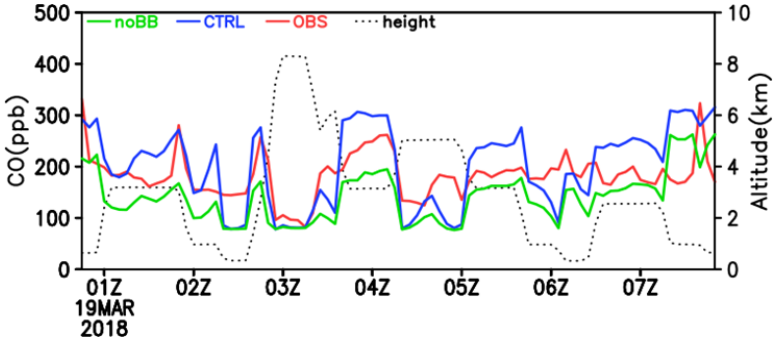

(b)

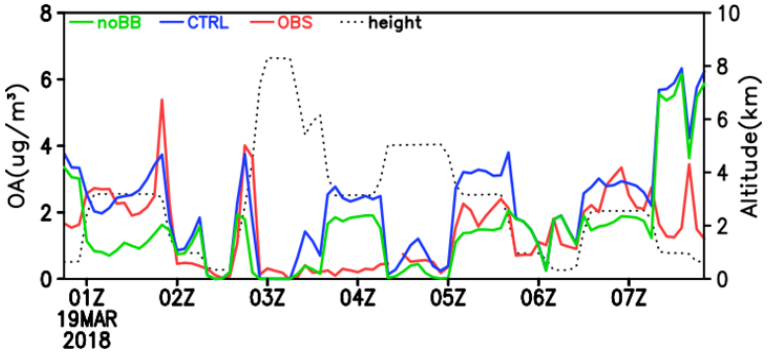

(c)

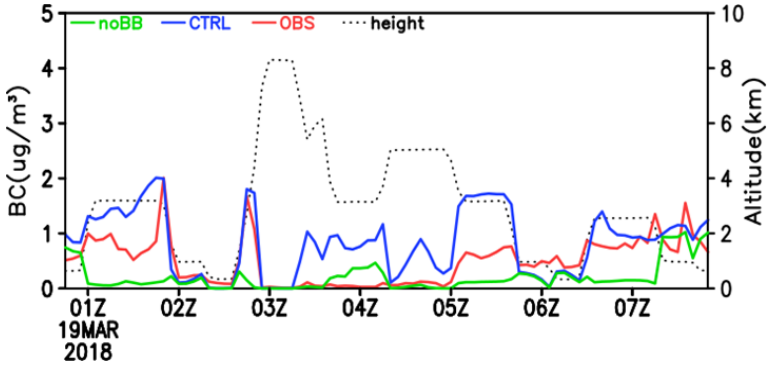

Fig.9 Observed (OBS, red) and simulated concentration with (CTRL, blue) and without (noBB, green) BB emission along with the flight altitude for (a) CO (ppb) (b) OA (μg m^{-3}) (c) BC (μg m^{-3}) on 19 March 2018.

https://doi.org/10.5194/acp-2022-517
Preprint. Discussion started: 9 August 2022

Atmospheric Chemistry and Physics Discussions

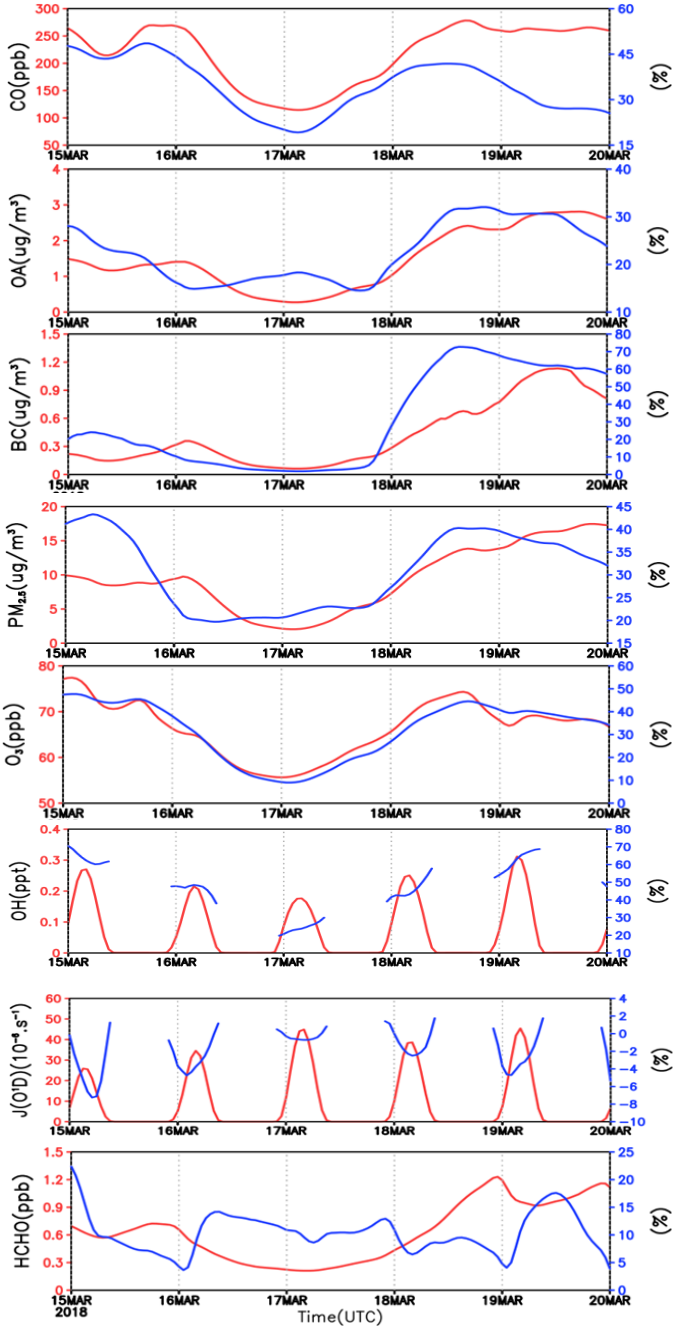

Figure 10 Hourly variation of simulated mean concentration (red) and contributed by BB (%, blue) between 2 km and 4 km over the region ECSA in Fig.1a during 15-19 March 2018. (a) CO (b) OA (c) BC (d) $PM_{2.5}$ (e)O_3 (f) OH (g) $J(O^1D)$, and (h) HCHO

https://doi.org/10.5194/acp-2022-517
Preprint. Discussion started: 9 August 2022

Atmospheric Chemistry and Physics Discussions

(a)

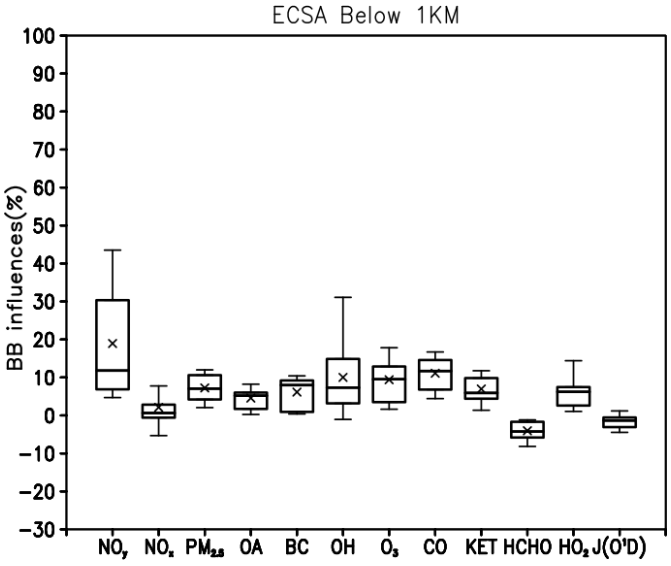

(b)

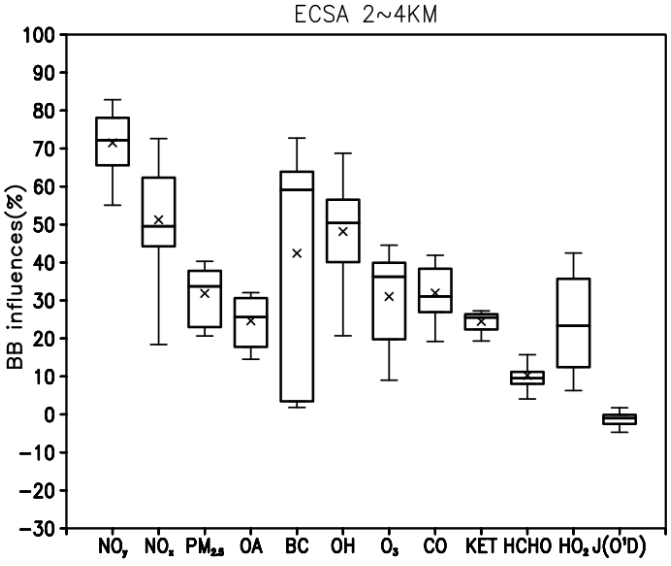

Figure 11 Box plots of simulated BB influences (%) on NO_y, NO_x, $PM_{2.5}$, OA, BC, OH, O_3, CO, KET, HCHO, HO_2 ,and $J(O^1D)$ over the region ECSA in Fig. 1a on 17 and 19 March 2018. (a) below 1 km, (b) between 2 km and 4 km

https://doi.org/10.5194/acp-2022-517
Preprint. Discussion started: 9 August 2022

Atmospheric Chemistry and Physics Discussions

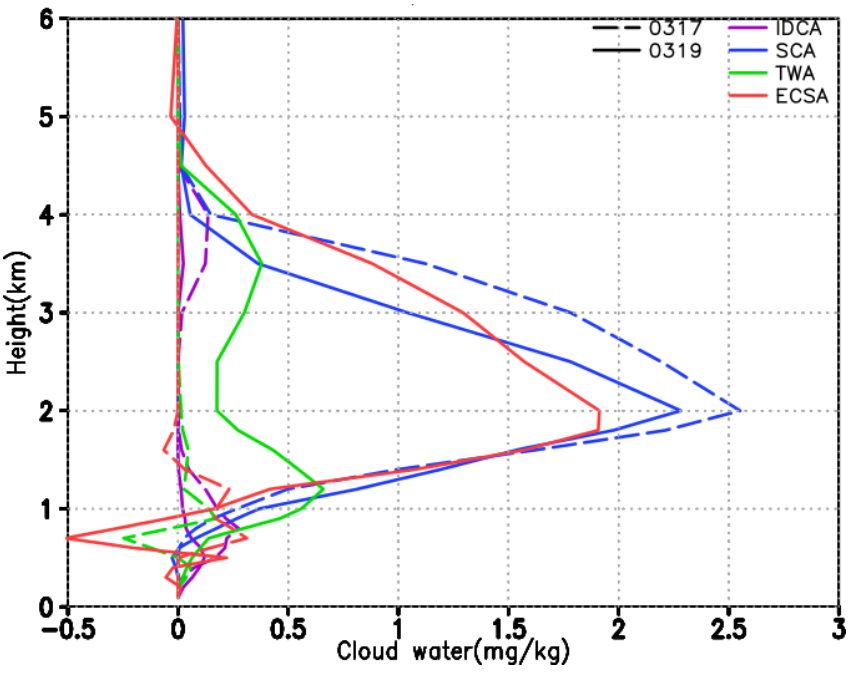

Figure 12 Simulated vertical distribution of BB influences on cloud water difference between with and without BB emission on 17 (dash) and 19 (solid) March 2018. Regions include IDCA, SCA, TWA, and ECSA as shown in Figure 1a.